ABSTRACT

Title of dissertation: FLAVORED DARK MATTER

Prateek Agrawal, Doctor of Philosophy, 2012

Dissertation directed by: Professor Zackaria Chacko
Department of Physics

Astrophysical observations point to the fact that most of the matter density in the universe is in the form of a non-luminous "dark matter". No particles detected so far satisfy the criteria to be dark matter candidates. If the present day dark matter density is set by thermal freeze out due to the expansion of the universe, then the dark matter particles likely have weak-scale interactions with ordinary matter. This opens up the possibility of detecting them in current experiments. We focus on a novel class of models – flavored dark matter – which contains multiple copies, or flavors, of dark matter particles, in analogy with the three copies of matter particles observed in nature. We classify such models and consider their implications for various dark matter searches. As an example, we choose one specific model with tau flavored dark matter, and consider its prospects for detection at the Large Hadron Collider.

FLAVORED DARK MATTER

by

Prateek Agrawal

Dissertation submitted to the Faculty of the Graduate School of the
University of Maryland, College Park in partial fulfillment
of the requirements for the degree of
Doctor of Philosophy
2012

Advisory Committee:
Associate Professor Zackaria Chacko, Chair/Advisor
Associate Professor Kaustubh Agashe
Associate Professor Paulo Bedaque
Professor Sarah Eno
Professor Alice Mignerey
Professor Raman Sundrum

Acknowledgments

This thesis is a result of help and support from many people. First and foremost, I would like to express deep gratitude towards my thesis advisor, Zackaria Chacko. He has always set high standards in every aspect of my graduate career, and helped me move towards meeting those standards. I owe him much of my understanding of particle physics through his lectures and numerous discussions with him. He has guided me to become a more competent physicist through collaborations on a number of projects.

I would like to thank Raman Sundrum for introducing me to the depth and beauty of quantum field theory through his lectures and many delightful conversations. He is a source of great inspiration for me. He has been always willing to take time out of his busy schedule to talk to me, which I truly appreciate. I have benefited immensely from his mentorship.

I thank Kevork Abazajian for advising me on my first project at Maryland, and for a very fruitful subsequent collaboration. I have enjoyed working with Can Kilic on a number of projects. I would like to thank him for teaching me many tricks of the trade. I would also like to thank Steve Blanchet, Ethan Dolle, Chris Krenke and Rashmish Mishra for fun and interesting collaborations. I have learnt a lot from my interactions with the faculty at the Maryland Center for Fundamental Physics. I would like to thank Kaustubh Agashe, Dr. Gates, Dr. Greenberg, Ted Jacobson and Rabi Mohapatra for their engaging lectures and conversations. I also thank other members of the particle physics group for many enjoyable discussions over the

years, Aleksandr Azatov, Yanou Cui, Roberto Francheschini, Anton de la Fuente, Andrey Katz, Doojin Kim, Takemichi Okui, Simón Riquelme, Matt Severson, Daniel Stolarski, Manuel Toharia, Chris Verhaaren, Kyle Wardlow and Lijun Zhu.

I would like to thank my co-inhabitants of the "international house of physics" – Jupiter Bagaipo, Dinko Ferenček, Zrinka Gregurić Ferenček, Ana Jesovnik, Kaushik Mitra, Juraj Radić, Marko Rajkovik, Kevin Schoeffler, Kanupriya Sinha and Yigit Subasi. They are part of many stories and fond memories that I will take with me from here.

I would like to express gratitude to Jane Hessing and Yuri Kubota. They have been very kind and have often gone out of their way to help me throughout my graduate career. There have been many more people who have provided indispensable help throughout these years, and I want to record my gratitude to all of them.

I am lucky to have a family who are immensely supportive and loving, and I owe all my achievements to them. My parents and my sister Pulak deserve my deepest gratitude.

I would lastly like to thank Katrin for reasons too many to put down here.

Table of Contents

List of Tables

List of Figures

List of Abbreviations

AMS	Alpha Magnetic Spectrometer
ATIC	Advanced Thin Ionization Calorimeter
BAO	Baryon Acoustic Oscillations
BBN	Big-Bang Nucleosynthesis
CDMS	Cryogenic Dark Matter Search
CKM	Cabibbo-Kobayashi-Maskawa
CMB	Cosmic Microwave Background
CoGeNT	Coherent Germanium Neutrino Technology
COUPP	Chicagoland Observatory for Underground Particle Physics
CP	Charge conjugation-Parity
CRESST	Cryogenic Rare Event Search with Superconducting Thermometers
DAMA/LIBRA	Dark Matter / Large sodium Iodide Bulk for RAre processes
DM	Dark Matter
FDM	Flavored Dark Matter
FLRW	Friedmann-Lemaître-Robertson-Walker
GC	Galactic Center
GeV	Gigaelectronvolt
GIM	Glashow-Iliopoulos-Maiani
HEAT	High Energy Anti-matter Telescope
KIMS	Korea Invisible Mass Search
KK	Kaluza-Klein
LAT	Large Area Telescope
ΛCDM	Lambda-Cold Dark Matter
LFDM	Lepton Flavored Dark Matter
LHC	Large Hadron Collider
MFV	Minimal Flavor Violation
MSSM	Minimal Supersymmetric Standard Model
PAMELA	Payload for Anti-matter Matter Exploration and Light-nuclei Astrophysics
QCD	Quantum Chromodynamics
QED	Quantum Electrodynamics
QFDM	Quark Flavored Dark Matter
SM	Standard Model
SN	Supernova
SUSY	Supersymmetry
τFDM	Tau Flavored Dark Matter
TeV	Teraelectronvolt
UED	Universal Extra Dimensions
VEV	Vacuum Expectation Value
WARP	WIMP Argon Programme

WIMP	Weakly Interacting Massive Particle
WMAP	Wilkinson Microwave Anisotropy Probe
ZEPLIN	ZonEd Proportional scintillation in LIquid Noble gases

Chapter 1

Introduction

Over the last century, we have pushed the boundaries of our understanding of the universe to ever larger and smaller distance scales. The Standard Model (SM) of particle physics describes phenomena remarkably well at the smallest distances probed till date. At the same time, the Lambda-Cold Dark Matter model (ΛCDM) of Big Bang cosmology fits astrophysical observations at the largest distance and time scales, explaining the evolution of the universe over most of its history.

Despite its many successes, the SM has a few limitations, which hint at the existence of new physics beyond the SM. The electroweak symmetry in the SM is broken by a scalar particle, the Higgs boson. The mass of a scalar is not protected by any symmetry, and is susceptible to corrections from physics at higher energy scales. If there is no new physics up to the Planck scale – where new physics must enter in the form of quantum gravity – we expect that the Higgs boson mass will generically get large corrections, of order the Planck scale, $m_{pl} \sim 10^{18}$ GeV. Existence of a light Higgs boson with mass around the TeV scale then requires a delicate fine-tuning among parameters. This is known as the hierarchy problem. If the SM is to be natural, we expect new physics near the TeV scale, the scale of electroweak symmetry breaking. The Large Hadron Collider (LHC) is a high energy collider at CERN designed to probe physics at the weak scale. It is currently taking

data, running proton-proton collisions at 8 TeV center-of-mass energy. The LHC has recently reported the discovery of a new particle, whose properties are those consistent those of the SM Higgs boson, with mass close to 125 GeV [3, 4]. It is hoped that the LHC will also find hints of new physics which makes the electroweak scale natural.

At the largest scales, analysis of the cosmic microwave background (CMB) radiation[5], predictions of baryon energy density [6], study of galactic rotation curves [7] and gravitational lensing [2] observations point to the fact that most of the matter density in the universe is in the form of a non-luminous "dark matter". The SM does not have a candidate particle which could make up this matter density. Even though there is a vast amount of astrophysical evidence for the presence of dark matter, the properties of the particles that make up the dark matter are largely unknown.

One simple and well-motivated possibility is that dark matter is made up of particles with masses close to the weak scale that have weak-scale annihilation cross section to Standard Model (SM) particles. Dark matter candidates with these properties neatly fit into the 'Weakly Interacting Massive Particle' (WIMP) paradigm and naturally tend to have the right relic abundance to explain observations. Since we expect new physics to appear around the weak scale, it is quite possible that dark matter particles are associated with this new physics.

In the rest of the chapter, we briefly introduce the elements of the Standard Model of particle physics, the Lambda-Cold Dark Matter model, and motivate WIMPs as dark matter candidates. We then introduce a novel class of dark matter

particles, called flavored dark matter, which form the central theme of this thesis. These models have new and interesting phenomenology in various experimental searches for dark matter. This thesis is based on work done in collaboration with Steve Blanchet, Zackaria Chacko and Can Kilic [8] and generally follows the presentation of that paper.

1.1 The Standard Model

The Standard Model of particle physics describes the electroweak and the strong nuclear forces of nature. The Standard Model is a gauge theory – these forces arise from exchanges of spin-1 particles, which are described by a local gauge invariant Lagrangian. Each force corresponds to its own local (gauge) symmetry group. Particles charged under a symmetry can exchange the corresponding spin-1 particles, the gauge bosons, and thereby exert force on each other.

The gauge group in the SM [9, 10, 11] is written as

$$SU(3)_C \times SU(2)_W \times U(1)_Y \ . \tag{1.1}$$

The gauge bosons form adjoint representations of their respective groups. The conserved charge of $SU(3)_C$, the strong nuclear charge, is denoted "color", and is mediated by gluons. The "weak" group $SU(2)_W$ has a triplet of gauge bosons, and the abelian group $U(1)_Y$ is called "hypercharge".

The SM is a chiral theory – matter particles possess specific handedness. Mat-

	$SU(3)_c$	$SU(2)_W$	$U(1)_Y$
Q^i	3	2	$\frac{1}{6}$
$(U^c)^i$	$\bar{3}$	1	$-\frac{2}{3}$
$(D^c)^i$	$\bar{3}$	1	$\frac{1}{3}$
L^i	1	2	$-\frac{1}{2}$
$(E^c)^i$	1	1	1

Table 1.1: Quantum numbers for Standard Model fermions.

ter fields in the SM are (left-handed) Weyl fermions[1], transforming under various representations of these gauge groups. The matter content of the SM is summarized in Table 1.1.

The matter particles charged under the color group are called quarks and the color singlets are called leptons. The index i denotes that there are three identical copies (referred to as flavors, generations or families) of matter particles in the SM. Independent rotations in flavor space for each fermion leave the gauge interactions and the fermion kinetic terms in the Lagrangian invariant. Thus, in addition to the gauge symmetries, the model described so far possesses an accidental $U(3)^5$ global flavor symmetry.

However, this model cannot be the end of the story. All fermion fields are chiral, and electroweak quantum numbers make it impossible to write mass terms

[1]Weyl fermions are 2-component spinor representations of the Poincaré group with definite chirality. A review can be found in [12].

for the matter fields at this level. Gauge invariance requires all the gauge bosons to be massless, which is at odds with observations of massive W and Z electroweak bosons. Therefore, electroweak symmetry must be broken.

One possibility is to simply write down the missing mass terms, and explicitly break electroweak symmetry. However, this would give up one of the grand achievements of the model – renormalizability. A theory of massive gauge bosons is not renormalizable, and breaks down at scales close to the gauge boson masses. If we introduce arbitrary new physics at this scale, we would lose much of the predictivity of the SM.

Renormalizability can be preserved if the electroweak symmetry is broken "spontaneously". The Lagrangian is constructed to be manifestly symmetric under the gauge symmetry, but the ground state of the theory does not respect the symmetry. Therefore, in excitations about this ground states, the gauge symmetry is not manifest. Remarkably, the proof of renormalizability of gauge theories applies to theories with spontaneous symmetry breaking [13].

In the Standard Model, the electroweak symmetry is spontaneously broken by the vacuum expectation value (VEV) of a scalar Higgs field. The potential for the Higgs field has a minimum at a constant non-zero value of the field. Since the Higgs field is charged under the $SU(2)_L \times U(1)_Y$ group (Table 1.2), a constant background value of the field breaks these symmetries. The Higgs VEV preserves a $U(1)_{QED}$ subgroup of the electroweak symmetry, and hence is neutral under electromagnetism.

The Higgs boson VEV sets the electroweak scale in the SM, and is equal to $v = 246$ GeV. The gauge boson mass eigenstates are linear combination of the

	$SU(3)_c$	$SU(2)_W$	$U(1)_Y$
H	1	2	$-\frac{1}{2}$

Table 1.2: Quantum numbers for Standard Model Higgs boson.

hypercharge and the $SU(2)_W$ gauge bosons. The massless eigenstate is the photon. The masses of the W and Z gauge bosons are given by [14],

$$m_W = \frac{1}{2} g v = 80.385 \pm 0.015 \text{ GeV} \tag{1.2}$$

$$m_Z = \frac{1}{2}\sqrt{g^2 + g'^2}\, v = 91.1876 \pm 0.0021 \text{ GeV}, \tag{1.3}$$

where g and g' are the $\mathrm{SU}(2)_W$ and the $\mathrm{U}(1)_Y$ coupling constants respectively.

We can now write down additional renormalizable terms – gauge invariant Yukawa couplings of the Higgs boson with the Standard Model matter fields,

$$\mathcal{L}_{mass} = y_j{}^i Q^j U_i^c H^\dagger + \hat{y}_j^i Q^j D_i^c H + \bar{y}_j^i L^j E_i^c H + \text{h.c.} \tag{1.4}$$

Here, $y, \hat{y}$ and $\bar{y}$ are three general complex-valued matrices. The indices i, j label flavor quantum numbers, and we have suppressed fermion and $SU(2)_W$ indices. The Higgs vacuum expectation value turns the Yukawa couplings into mass terms for fermions. Hence the masses for fermions are determined by their couplings with the Higgs boson.

These couplings are the only source of explicit violation of the accidental flavor symmetries of the SM. Hence, flavor violation in the SM is encoded in the Yukawa matrices. The mass terms can be diagonalized using flavor rotations. The quark mass terms can be diagonalized by rotating Q, U^c and D^c fields. The QCD, QED

and Z couplings are diagonal in flavor space, so that the effect of non-diagonal Yukawa couplings only appears as in the W couplings of Q^i, in the form of the Cabibbo-Kobayashi-Maskawa (CKM) matrix [15, 16]. All flavor violation is then encapsulated in the CKM matrix.

Since the photon and Z boson couplings stay diagonal under this rotation, there are no flavor-changing neutral currents at tree level in the SM. They arise at one loop level, and are further suppressed as a consequence of the unitarity of the CKM matrix. This suppression is known as the Glashow-Iliopoulos-Maiani (GIM) mechanism [17]. Further, the presence of the 3×3 CKM matrix admits one phase which cannot be absorbed in field redefinitions. This is a consequence of the fact that the SM has a residual $U(1)_B$ symmetry, the baryon number, responsible for the stability of the proton. This phase is responsible for CP violation in the SM.

One can perform similar flavor rotations in the lepton sector. Ignoring the effects of small neutrino masses, the absence of singlet neutrinos allows us to diagonalize the lepton mass matrices without introducing additional mixing in the gauge couplings. Therefore, the lepton sector in the SM preserves an approximate $U(1)^3$ symmetry – at zeroth order in neutrino masses, there are no flavor-changing processes in the lepton sector of the SM.

Generically, new physics will introduce new sources of flavor and CP violation. Many different flavor observables put stringent bounds on these contributions, such that $\mathcal{O}(1)$ flavor violation can only arise from scales much higher than the weak scale (100-10000 TeV [18]). Therefore, new physics at the weak scale cannot have a generic flavor structure, but must conform to the SM patterns of flavor violation.

This is not entirely implausible, since we currently have no explanation for the flavor structure in the SM, and it is possible that the physics which imparts flavor structure to the SM also imparts it to the new physics at the weak scale.

The flavor structure of the SM will play a major role in our discussion of flavored dark matter.

1.2 Lambda-Cold Dark Matter

The Lambda-Cold Dark Matter model is a cosmological model describing the evolution of the universe in its early phases, the existence and the features of the CMB, the development of large scale structures (such as galaxies, galaxy clusters) and relative abundances of various light elements.

The CMB provides us with many of the clues that help us deduce the evolution and current state of the universe. In the early universe there was enough energy to disassociate hydrogen atoms into a charged plasma state. As the universe cooled down, electrons and protons recombined to form hydrogen, and the universe became transparent to photons, which form the CMB observed today. The temperature and density of the plasma at the time of recombination are imprinted on the CMB, and yield valuable information about the early universe.

One of the key observations is that the universe is observed to be approximately isotropic. The CMB has a uniform black body spectrum with temperature around 2.7 K, with tiny variations of 1 part in 10^5 (Fig. 1.1). Isotropy, coupled with the "Copernican principle" that every point in the universe is equivalent (aided with

some evidence from counting galaxies), leads to the conclusion that the universe is spatially homogeneous.

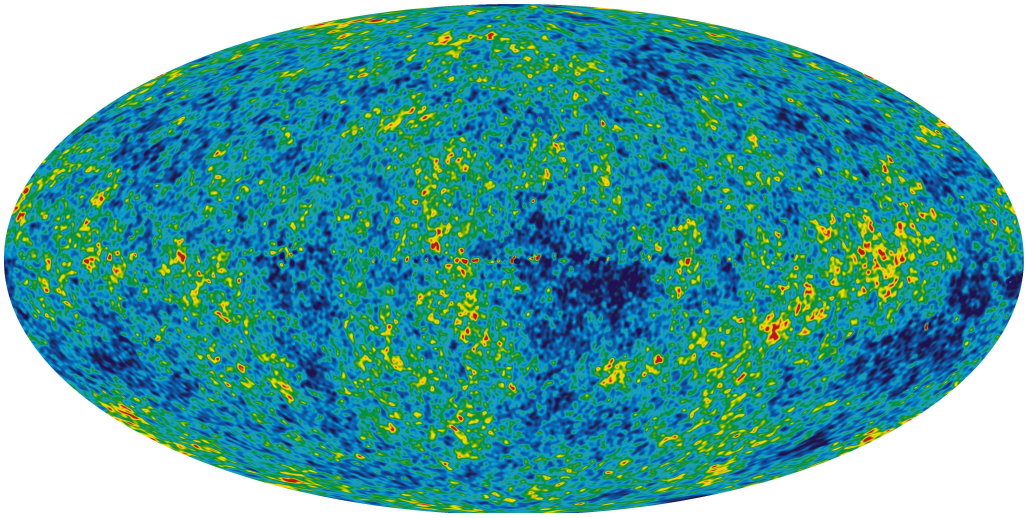

Figure 1.1: The cosmic microwave temperature fluctuations from the 5-year WMAP data seen over the full sky. The average temperature is 2.725 Kelvin, and the colors represent the tiny temperature fluctuations. Red regions are warmer and blue regions are colder by about 0.0002 degrees [19].

The geometry of a isotropic and homogeneous universe is given by the Friedmann-Lemaître-Robertson-Walker (FLRW) metric,

$$ds^2 = dt^2 - a^2(t)\left[\frac{dr^2}{1-kr^2} + r^2(d\theta^2 + \sin^2\theta d\phi^2)\right], \tag{1.5}$$

where $k = +1, 0, -1$ corresponds to a spatially closed, flat or open universe. The CMB data strongly indicates that our universe is spatially flat. The metric above uses co-moving coordinates. The dynamics of spacetime are encoded in the scale-factor $a(t)$, and galaxies keep fixed coordinates in the absence of external forces acting on them. Physical distances are obtained by multiplying with the scale

factor, $R = a(t)r$. The Hubble parameter H is defined as,

$$H \equiv \frac{\dot{a}}{a}. \tag{1.6}$$

Einstein's equations of General Relativity lead to the following equation for the scale factor,

$$\left(\frac{\dot{a}}{a}\right)^2 = \frac{1}{3m_{pl}^2}\sum_i \rho_i - \frac{k}{a^2}, \tag{1.7}$$

where ρ_i is the energy density of component i. We define critical density as the energy density at any given time for which the above equation is satisfied for $k = 0$. Thus, the critical density is given by,

$$\rho_c = 3H^2 m_{pl}^2. \tag{1.8}$$

The Planck mass is defined to be $m_{pl} \simeq 2 \times 10^{18}$ GeV.

Then, the total energy density can be expressed as a ratio with respect to the critical density,

$$\Omega_{total} \equiv \frac{\rho}{\rho_c}. \tag{1.9}$$

Clearly, the condition for a flat universe then is that the sum of energy densities of each component should be equal to 1,

$$\sum_i \Omega_i = 1. \tag{1.10}$$

The CMB provides some of the most effective tools to study the relative contributions of various components. The temperature fluctuations in the CMB reflect the temperature and density variations of the plasma at the time of recombination. Since regions of different density have different gravitational potential, these

cause different redshifts for photons, which result in anisotropies in the CMB. The power spectrum of the CMB measures the size of these anisotropies, decomposed in spherical harmonics (Fig. 1.2).

An overdense region collapses over a time-scale of its size. If the size of this region is much larger than the age of the universe at recombination (in units where $c = 1$), it would not have had enough time to collapse. On the other hand, if the size is much smaller than the age of the universe, it would have collapsed by the time of last scattering and the resulting photon pressure would damp out the inhomogeneity. Therefore, the typical size of density fluctuation would be the $R \sim H_{CMB}^{-1}$, which is the age of the universe in a matter-dominated universe. Thus, we can deduce the spatial curvature of the universe by comparing the angular size of typical density fluctuations and H_{CMB}^{-1}. The CMB strongly hints at a flat universe, $\Omega_{total} = 1$, based on the peak in the power spectrum at $l \simeq 220$ (Fig. 1.2).

The components making up most of the energy density of the universe today are the cosmological constant Ω_Λ and the matter density Ω_m. The matter density has two contributions, the dark matter Ω_{DM} and baryonic matter Ω_b. Other forms of ordinary matter (electrons, neutrinos, photons) contribute only a small fraction ($\lesssim 1\%$) of the total energy density.

There are many independent measurements of different combinations of these components. We briefly describe a few main observations which help in fixing the parameters of the ΛCDM model.

Type 1a supernovae (SNe) result from explosion of a white dwarf star, and have a characteristic light curve. They serve as "standard candles" and are bright enough

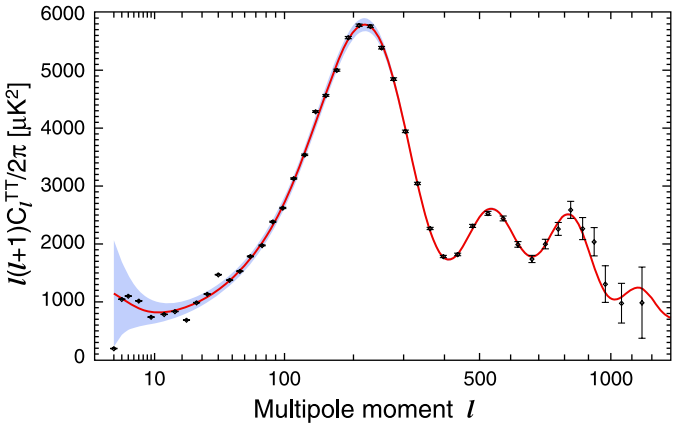

Figure 1.2: The 7-year temperature power spectrum from WMAP. The curve is the ΛCDM model best fit to the 7-year WMAP data. The plotted errors include instrument noise, but not the small, correlated contribution due to beam and point source subtraction uncertainty. The gray band represents cosmic variance [5].

to be detected at high redshifts, allowing a probe of the early universe cosmology. A study of distant supernovae to measure cosmological parameters shows that the SNe data are much better fit by a universe dominated by vacuum energy, an energy density which does not get diluted with the expansion of space. The discovery of the accelerated expansion of the universe was awarded the Nobel Prize in Physics 2011 [20, 21, 22].

Baryon Acoustic Oscillations (BAO) provide independent "standard rulers" on the sky, by comparing the sound horizons today (from measurements of clustering of galaxies) to the sound horizon at the time of recombination (using the CMB) [23].

The amount of baryons in the universe can be estimated by a variety of methods: direct counting of baryons, CMB anisotropies and predictions of light element abundances from Big Bang nucleosynthesis (BBN) [6]. The baryon energy density

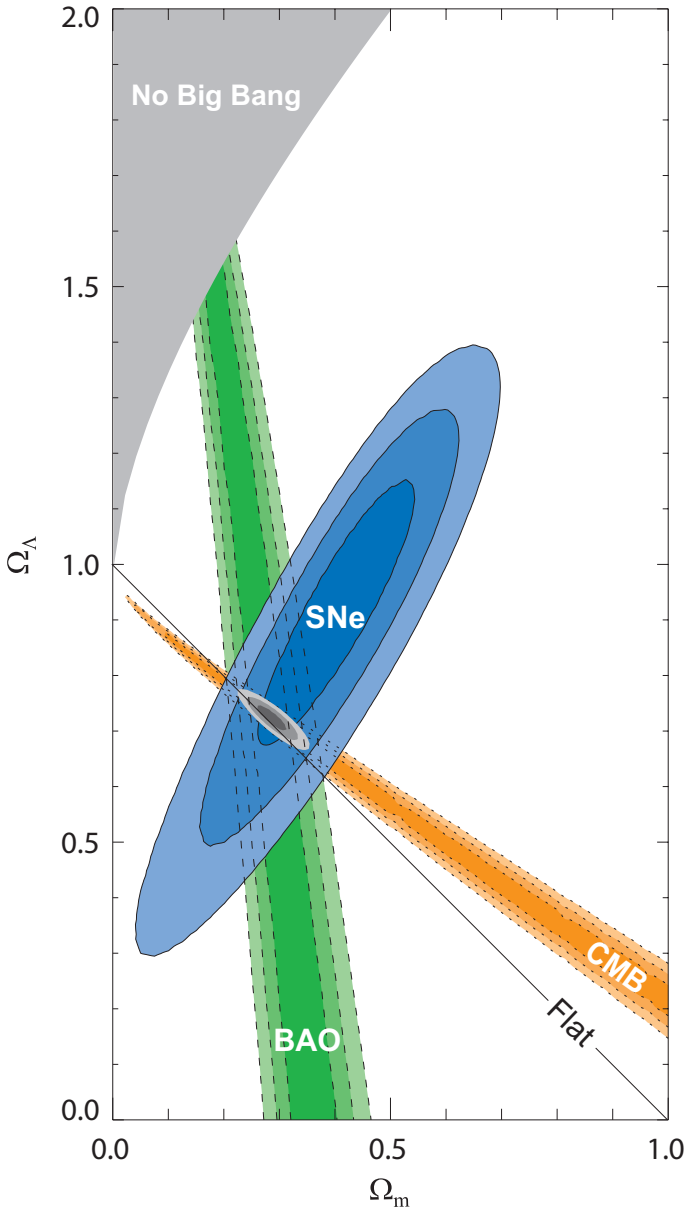

Figure 1.3: 68.3 %, 95.4 % and 99.7% confidence level contours on Ω_Λ and Ω_m obtained from CMB, BAO and the Union SN set, as well as their combination (assuming $w = -1$) [24].

Parameter	WMAP+BAO+H0 Mean
H	70.2 ± 1.4 km/s/Mpc
Ω_Λ	0.725 ± 0.016
Ω_b	0.0458 ± 0.0016
Ω_{DM}	0.229 ± 0.015
t_0	13.76 ± 0.11 Gyr

Table 1.3: Summary of relevant parameters in the Lambda-Cold Dark Matter model [5]

predicted by various methods is consistent within the ΛCDM framework, and is only around 4.5% of the total energy density.

Together, these observations define the ΛCDM parameters or concordance cosmology (Fig. 1.3). The best fit parameters in the ΛCDM model from WMAP observations are summarized in Table 1.3.

Therefore, most of the matter density is made up of a non-baryonic, or a "dark" component, called "dark matter". There are no candidates for this dark matter in the SM and therefore, evidence for dark matter is direct evidence for physics beyond the SM.

The dark matter should remain non-relativistic (hence "cold") for much of the history of the universe. If the dark matter were relativistic, it would free-stream out of overdense regions, suppressing structure formation. This puts a lower bound on the dark matter mass, $m_{DM} \gtrsim$ keV [25].

Recently there has been a direct cosmological observation of dark matter in the "bullet cluster" (Fig. 1.4) [2]. Most of the baryonic matter in the cluster is in the form of a hot gas which emits X-rays. The X-ray emissions form a bullet

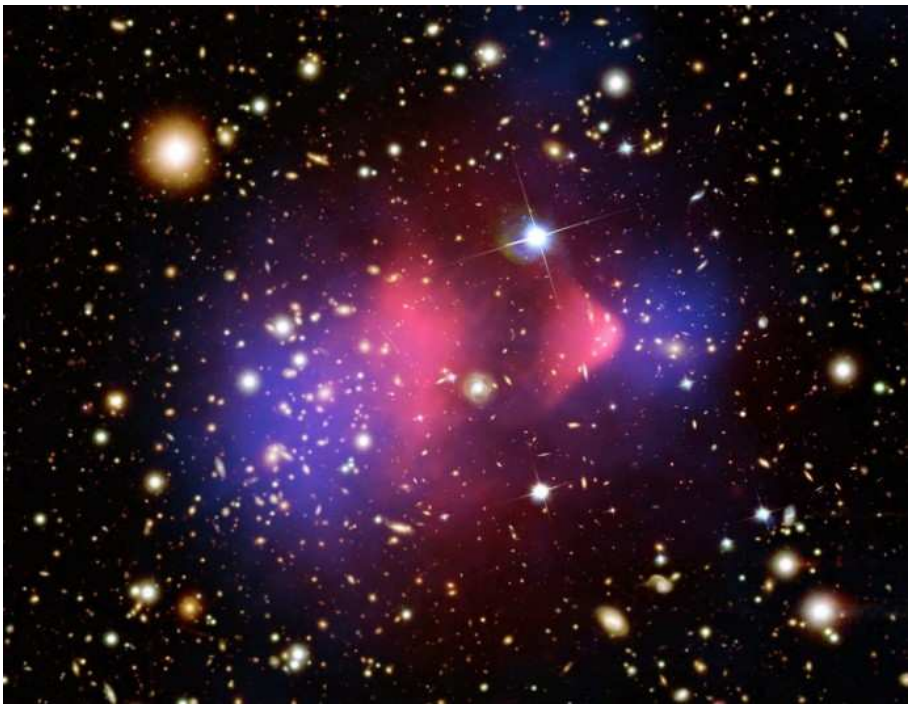

Figure 1.4: A composite image of the bullet cluster. The pink region denotes X-rays observed by the Chandra X-ray observatory [1]. The blue regions indicate the concentration of mass as deduced by weak gravitational lensing of background galaxies [2]. An optical image from Magellan and the Hubble Space Telescope shows the galaxies in orange and white.

shaped shock-front, arising from a primordial collision between two galaxy clusters. However, most of the mass in the cluster deduced from weak gravitational lensing observations is shown to be separated from this shock front. The interpretation is that most of the matter in the galaxy cluster is in dark matter haloes, which interact very weakly through gravity and hence are separated from ordinary matter during the collision.

We see that there is a very strong case for the existence of dark matter from many independent astrophysical observations. However, none of these observations

probe the interaction of dark matter particles with SM particles beyond gravity. If dark matter particles are thermal relics, they automatically have the correct relic abundance ($\Omega_{DM} \simeq 0.23$) if they have weak-scale interactions with ordinary matter. We study this aspect in more detail below.

1.3 Relic Abundance of Dark Matter

A universe described by the FLRW metric does not possess an equilibrium state. Our universe has been steadily expanding throughout its history. However, on timescales much shorter than the expansion, the universe can be approximated to be quasi-static.

The photon bath in the early universe has a black body spectrum. As the universe expands, the photons red-shift, but they maintain a black body spectrum at a lower temperature. Therefore, the universe can be described as a black body plasma (comprised of the relativistic species), which cools down as the universe expands.

If all components in the universe stayed in thermal equilibrium, we would be left with a featureless 2.7 K universe today. The departures from thermal equilibrium are very important to the history of the universe and the subsequent structure formation.

If the dark matter (denoted henceforth by the symbol χ) is a thermal WIMP, its relic abundance is set by its annihilation rate to SM fields. Dark matter particles are kept in thermodynamic equilibrium when the annihilations and inverse processes

are fast compared to the expansion of the universe. Once the annihilation rate of dark matter drops below the expansion rate, it no longer remains in chemical equilibrium, and its number density effectively "freezes out". Subsequently, its number density per co-moving volume does not change, and the density at freeze-out sets the relic abundance of that dark matter.

We briefly outline the relic abundance calculation in this chapter. A more detailed analysis is postponed to Chapter 3. The freeze out occurs at a temperature where the annihilation rate of dark matter becomes comparable to the expansion rate of the universe.

$$\langle \sigma v \rangle n_{eq} = H. \tag{1.11}$$

where n_{eq} is the number density of dark matter particles at a given temperature when they are in thermal equilibrium.

The freeze out temperature depends logarithmically on the annihilation cross section, mass and spin of the dark matter. For typical weak scale values, Eq. 1.11 defines the freeze out temperature $x_f \sim 20$, where $x = m_\chi/T$.

The dark matter density after the annihilations become inefficient is well approximated by $n_{eq}(x_f)$, the equilibrium density at freeze out. The co-moving relic density can be obtained by using the entropy density s as a fiducial volume. After freeze out, the dark matter density normalized by the entropy density, n_χ/s, remains constant. The present day dark matter energy density is given by,

$$\Omega_{DM} = \frac{m_\chi n_\chi(x_0)}{\rho_c(x_0)} = \frac{m_\chi}{\rho_c(x_0)} s(x_0) \frac{n_{eq}(x_f)}{s(x_f)} \simeq 0.23 \, \frac{3 \times 10^{-26} \text{ cm}^3/\text{s}}{\langle \sigma v \rangle} \, . \tag{1.12}$$

In calculation of the relic density, particle physics parameters enter only through the annihilation cross section and the freeze out temperature, x_f. Since the freeze out temperature is largely independent of dark matter mass and spin, the dark matter relic abundance is dominantly set by the annihilation cross section. From Eq. 1.12, we see that

$$\langle \sigma v \rangle \sim 3 \times 10^{-26} \text{ cm}^3/\text{s} \tag{1.13}$$

yields the correct relic abundance. This is a cross section expected from a weak-scale interaction. For comparison, the Fermi constant G_F for weak interactions is given by,

$$G_F = \frac{\sqrt{2}}{8} \frac{g^2}{m_W^2} \simeq 1.4 \times 10^{-24} \text{ cm}^3/\text{s}. \tag{1.14}$$

in units where $\hbar = c = 1$. Therefore, an interaction mediated by a TeV scale particle automatically yields the correct relic abundance of dark matter. This is known as the WIMP miracle, and suggests that it might be possible to detect dark matter in current experiments.

1.4 Detection of Dark Matter

In this section we describe various experimental searches for dark matter particles. While there have been a few tantalizing hints, there are currently no definitive signals of dark matter in any particle physics experiment.

Each class of experiment focuses on a complementary aspect of dark matter physics. We study each class in detail below.

1.4.1 Direct Detection

Direct detection experiments are designed to observe nuclear recoils when a dark matter particle scatters off it. There are a number of experiments searching for dark matter - nucleus interactions: CDMS [26], Xenon [27], ZEPLIN [28], EDELWEISS [29], CRESST [30], CoGeNT [31], DAMA/LIBRA [32], COUPP [33], WARP [34] and KIMS [35].

The typical nuclear recoil energy in a scattering event is

$$E_{recoil} = \frac{|\vec{q}|^2}{2m_{nuc}} \sim m_{nuc}\frac{m_\chi^2 v^2}{(m_\chi + m_{nuc})^2}. \tag{1.15}$$

For typical WIMP and detector nuclei masses ($m_\chi \sim m_{nuc} \sim 100$ GeV), and typical WIMP halo velocity $v \sim 300$ km/s [36], the recoil energy is $E_{recoil} \sim 100$ keV.

Fig. 1.5 shows a typical constraint plot from direct detection experiments. The experimental sensitivity is poor for low mass WIMPS ($m_\chi \lesssim 10$ GeV), because the typical recoil energy for these particles lies below the energy thresholds for experiments. This explains the sharp weakening of the limit towards small dark matter masses. For dark matter particles with mass $m_\chi \gtrsim 1$ TeV, the number density (and hence the interaction rate) starts decreasing, leading to a gradual weakening of limits for high mass dark matter.

Apart from the mass and the scattering cross section, the rate of events in direct detection is sensitive to astrophysical parameters, including the local dark matter density and the velocity distribution of dark matter particles in our neighborhood. Nuclear matrix elements of various quark bilinears also affect the rates, and are known reliably in most but not all cases of interest.

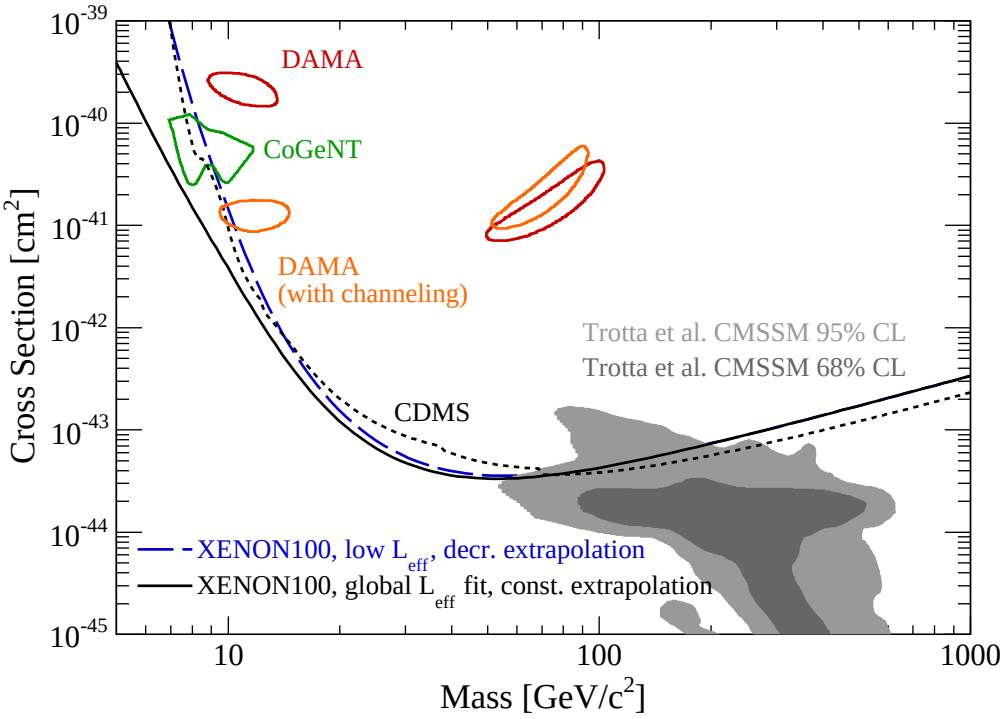

Figure 1.5: 90% confidence limit on the spin-independent elastic WIMP-nucleon cross section (solid and long dashed)[37], together with the best limit to date from CDMS (dotted) [26], recalculated assuming an escape velocity of 544 km/s and $v_0 = 220$ km/s. Expectations from a theoretical model [38], and the areas (90% CL) favored by CoGeNT (green) [31] and DAMA (red/orange) [39] are also shown.

The cross section for WIMPs to scatter off different nuclei depends strongly on the form of the interactions of the dark matter particle. The momentum transfer in scattering processes is smaller than typical nuclear energy scales, so the WIMP scatters off the nucleus as a whole. If the dark matter couples to the mass (or charge) of the nucleus, the event rate increases dramatically for heavier nuclei. This is one of the reasons to employ heavy nuclei in direct detection experiments. These interactions are known as spin-independent interactions. In contrast, the spin of the nucleus is much smaller than the number of nucleons in the nucleus. Therefore, spin-dependent interactions lead to much smaller event rates.

The bounds on WIMP-nucleus scattering from direct detection experiments are generally expressed as limits on the WIMP-nucleon cross section in order to allow comparing results across experiments using different nuclei. The bounds are different if one assumes spin-independent or spin-dependent scattering. Clearly, the bounds on WIMP-nucleon scattering assuming spin-dependent interactions are relatively weak since the spin of a typical nucleus is either zero or order one, and does not scale with A, the number of nucleons. On the other hand, spin-independent cross sections are enhanced by a factor of A^2 , and the bounds on such interactions are correspondingly stronger by a factor of order 10^5.

1.4.2 Indirect Detection

Another class of dark matter searches attempts to detect products of WIMP annihilation, including photons, positrons and electrons, anti-protons and neutrinos.

The rate of annihilation for WIMPs in the early universe is set by the requirement that they be thermal relics, i.e. $\langle \sigma v \rangle \sim 3 \times 10^{-26}$ cm^3/s. If this cross section is temperature independent (s-wave), the same rate applies to present day annihilation in the halo.

This scale predicts a potentially detectable gamma-ray photon signal from annihilations in local and cosmological dark matter structures, see [40, 41]. Annihilation channels directly to photon pairs produce a distinctive ray spectral line, while channels to charged SM particles produce an associated continuum emission of γ-rays from bremsstrahlung radiation and in hadronization via $\pi^0 \to \gamma\gamma$. The Large Area Telescope (LAT) aboard the recently launched Fermi Gamma-Ray Space Telescope has significant sensitivity to such γ-ray radiation from dark matter annihilation. The sensitivity of Fermi-LAT to an annihilation signal from the Galactic center (GC), Galactic satellites and the isotropic diffuse signal was reviewed in Baltz et al. [42]. Recently, there have been indications of a line feature in the photon spectrum observed by Fermi-LAT [43, 44]. If confirmed, the line spectrum would very likely have a dark matter origin, and would constitute the first detection of dark matter particles.

Annihilation to various other final states such as electrons, positrons and antiprotons also leave their signature on the cosmic ray spectrum. Since charged particles curve in the Galactic Magnetic Field and lose energy, the signal observed at the Earth is diffuse and smeared. Consequently, it is harder to distinguish between astrophysical sources and dark matter as the origin of such a signal. The PAMELA experiment [45] reported an excess in the cosmic ray positron fraction (ratio of

positron events to positron and electron events). This confirmed an earlier result by HEAT [46] and AMS-01 [47]. A balloon-based experiment, ATIC [48] also reported a rising feature in cosmic ray electron spectrum. Recently the Fermi-LAT experiment has found results for the cosmic ray positron fraction which are consistent with the PAMELA findings [49]. These signals could arise from dark matter annihilation, with a "boosted" rate of annihilation relative to the thermal relic prediction. This boost could arise from a particle physics or an astrophysical source. These signals are also consistent with a electron-positron emission from nearby pulsars (see for example [50]).

Neutrino telescopes seek to detect high energy neutrinos from dark matter annihilation. Dark matter can scatter off nuclei in celestial bodies like the Sun into a gravitationally bound orbit. After subsequent scattering, it can accumulate in the center of these bodies and annihilate with other dark matter particles. Over the lifetime of the solar system, a sufficient density of dark matter particles can accumulate so that the capture and annihilation processes are in equilibrium. If the annihilation products of dark matter yield high energy neutrinos, these neutrinos escape from the Sun and can be potentially detected in neutrino telescopes on Earth, such as IceCube [51] and Super-Kamiokande[52].

In equilibrium, the annihilation rate is set by the capture rate, which is in turn set by the WIMP-nucleon scattering cross section. Since the Sun is made up predominantly of hydrogen, spin-independent scattering is only moderately enhanced over spin-dependent scattering, and they lead to comparable bounds. The strongest bounds on spin-independent scattering arise from direct detection experiments, but

for certain spin-dependent models, the strongest bounds on WIMP-nucleon scattering arise from neutrino observatories like IceCube and Super-Kamiokande [53].

1.4.3 Collider Signatures

The direct and indirect detection experiments are sensitive to many astrophysical uncertainties and backgrounds. In such a case, it is an attractive possibility to create dark matter particles in high energy colliders and deduce their microscopic properties.

In many models of beyond the Standard Model Physics, dark matter particles arise as parts of extended sectors which have interactions with the SM particles. Particles mediating interactions between the SM and dark matter can then be produced directly at high energy colliders if they are kinematically accessible. These could then decay into visible SM particles and the dark matter particles. The dark matter particles escape detection, but their production can be deduced by measurement of final state momentum imbalance. Such a "missing energy" signal is a common signature of most dark matter searches at colliders.

The physics of electroweak symmetry breaking is currently being probed at the LHC. As the experiment collects more data at higher energies in the future, it is hoped that it will produce new TeV scale particles, including those associated with dark matter.

A robust model independent bound can be established on direct dark matter production by observation of photons from initial state radiation with missing energy

[54]. Other specific collider signatures of dark matter largely depend on the new physics sector associated with it. If there are accessible colored states in the "dark sector", these can be copiously produced at a hadron collider, leading a large event rate. At the same time, the background for colored final states is large, and the backgrounds for leptons are well understood. Hence, models which predict visible leptonic final states can still be probed effectively, even if the production rate is smaller. In chapter 5 we will consider one particular example of a model of dark matter with tau flavor and analyze its prospects for detection at the LHC.

1.4.4 Axion Dark Matter Experiments

A possible alternative to the WIMP hypothesis is axion dark matter. The axion was initially introduced as a solution to the strong CP problem in the SM. The following term is allowed by all the symmetries of the SM,

$$\frac{g_s^2}{32\pi^2}\theta_{QCD}\ tr[G\widetilde{G}]\,, \tag{1.16}$$

where g_s is the strong coupling and G is the gluon field strength. Consequently, we expect the θ_{QCD} parameter to be order unity. However, experimental observations limit the $\theta_{QCD} \lesssim 10^{-10}$.

A solution to the strong CP problem is obtained by elevating θ_{QCD} to a dynamical field, which is set to zero over the cosmological timescales by its potential [55, 56, 57, 58, 59, 60, 61, 62]. This field arises as a pseudo-Nambu Goldstone boson associated with the spontaneous breaking of an approximate $U(1)$ symmetry. If the axion field is misaligned from its minimum initially, it subsequently oscillates

coherently about this minimum, contributing to the cosmological energy density as dark matter [63, 64, 65].

The energy density of the axion depends on its decay constant, f_a. For large initial misalignment, the decay constant is required to satisfy $f_a \lesssim 10^{12}$ GeV. Astrophysical bounds put a lower bound, $f_a \gtrsim 10^9$ GeV. There are experiments probing the region 10^{10} GeV $\lesssim f_a \lesssim 10^{12}$ GeV using conversion of the axion to microwave radiation in the presence of a background magnetic field [66, 67]. There have also been novel proposals to probe other regions of the axion parameter space using astrophysical observations [68] and time-varying shifts in atomic energy levels [69].

1.5 Flavored dark matter

The matter fields (Q, U^c, D^c, L, E^c) of the SM have three copies, or flavors, that differ only in their masses. This reflects the fact that the Lagrangian of the SM possesses an approximate $\mathrm{U}(3)^5$ flavor symmetry acting on the matter fields, which is explicitly broken by the Yukawa couplings that generate the quark and lepton masses. An interesting possibility is that the dark matter field χ, also carries flavor quantum numbers, with the physical dark matter particle being the lightest of three copies. Several specific dark matter candidates of this type have been studied extensively in the literature, including sneutrino dark matter [70, 71, 72, 73, 74, 75] (for recent work see [76]) in the Minimal Supersymmetric Standard Model (MSSM), and Kaluza-Klein (KK) neutrino dark matter [77] in models with a universal extra dimension (UED). Other realizations of flavored dark matter that have received recent study

include theories where dark matter couples primarily to quarks, potentially giving rise to interesting flavor violating signals [78, 79]. It has also been shown that flavored dark matter may play a role in explaining the baryon asymmetry [80], and that extending the SM flavor structure to the dark sector can explain the stability of dark matter [81].

To incorporate three flavors of the dark matter field, the flavor symmetry of the SM is extended from $U(3)^5$ to $U(3)^5 \times U(3)_\chi$, if χ is a complex field such as a complex scalar, Dirac fermion or complex vector boson. If instead χ is a real field, such as a real scalar, Majorana fermion or real vector boson the flavor symmetry is extended from $U(3)^5$ to $U(3)^5 \times O(3)_\chi$. The new flavor symmetry $U(3)_\chi$ (or $O(3)_\chi$) may be exact, or it may be explicitly broken as in the SM.

Our focus will be on theories where dark matter has renormalizable contact interactions with the SM fields. Consider first the case where these contact interactions include couplings to the SM matter fields. These must be of the form shown in Fig. 1.6(a). If the dark matter flavor symmetry is to be exact, the field ϕ that mediates this interaction must transform under $U(3)_\chi$ (or $O(3)_\chi$). If this vertex is to respect the SM flavor symmetry, ϕ must also transform under the SM flavor group. In such a scenario, the different flavor states in the dark matter multiplet are degenerate, and the observed dark matter in the universe will in general consist of all three flavors. Alternatively, this contact interaction, in analogy with the SM Yukawa couplings, could represent an explicit breaking of the flavor symmetry. It is this scenario that we will be primarily concerned with in this thesis. In this case the simplest possibility is that the mediator ϕ is a singlet under both the SM and the

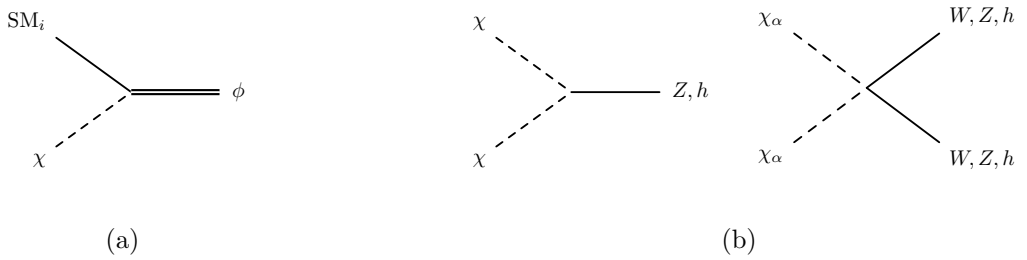

Figure 1.6: Vertices that link dark matter to a) the SM matter fields and b) the SM gauge and Higgs fields.

dark matter flavor groups. Then, if the SM matter field that χ couples to is a lepton, there is an association between the different dark matter flavors and lepton flavors. Accordingly, we refer to this scenario as 'lepton flavored dark matter'. Sneutrino dark matter and Kaluza-Klein neutrino dark matter are special cases that fall into this category, as does the model of [80]. Similarly, we label the corresponding case where χ couples to a quark as 'quark flavored dark matter'. The models of flavored dark matter studied in [79] fall into this category. In this framework the fact that the SM flavor symmetries are not exact naturally results in a splitting of the states in the dark matter multiplet, the physical dark matter particle being identified with the lightest.

A different class of theories involves models of flavored dark matter where direct couplings between χ and the SM matter fields at the renormalizable level are absent. Instead, the contact interactions of χ with SM fields are either with the W and Z gauge bosons, or with the Higgs, and can naturally preserve both the SM flavor symmetries and the dark matter flavor symmetry. The general form of such vertices is shown in Fig. 1.6(b). Closely related to this are theories with interactions

of the exactly same form, but where dark matter instead couples to a new scalar ϕ or vector boson Z', which then acts as a mediator between the SM fermions and the dark sector. The model of flavored dark matter studied in [78] falls into this category. In such a framework, dark matter is in general not associated with either quark or lepton flavor. We therefore refer to this scenario as 'internal flavored dark matter'.

Since the characteristic vertices of lepton flavored, quark flavored and internal flavored dark matter are distinct, their implications for phenomenology are very different. In the next chapters we consider each of these classes of theories in detail, and study their collider signals, as well as their implications for direct detection and flavor physics. We then focus on a specific model of tau flavored dark matter and show that its collider signals include events with four or more isolated leptons and missing energy that can allow these theories to be discovered at the LHC above SM backgrounds. We also study the extent to which flavor and charge correlations among the final state leptons allows models of this type to be distinguished from more conventional theories where the dark matter particle couples to leptons but does not carry flavor, such as neutralino dark matter in the MSSM.

Chapter 2

Flavor Structure

New sources of flavor violation beyond the SM are severely constrained by a number of low-energy experiments. Therefore, new couplings of dark matter with SM matter cannot be arbitrary, but must fit the pattern of flavor violation in the SM [18].

All flavor violation in the SM arises from the Yukawa couplings of the fermions with the Higgs boson. Couplings of dark matter to SM fermions must then be aligned with Yukawa matrices to preserve the flavor structure of the SM. One way to achieve this is to work in the framework of Minimal Flavor Violation (MFV) [82]. We discuss the possible flavor structure of flavored dark matter (FDM) in detail below.

2.1 Lepton Flavored Dark Matter

We first consider the case where dark matter carries lepton flavor. The lepton sector of the SM has a $\mathrm{U}(3)_L \times \mathrm{U}(3)_E$ flavor symmetry, where $\mathrm{U}(3)_L$ acts on the $\mathrm{SU}(2)_W$ doublet leptons and $\mathrm{U}(3)_E$ on the singlets. This symmetry is explicitly broken down to $\mathrm{U}(1)^3$ by the Yukawa interactions that give the charged leptons their masses. (We neglect the tiny neutrino masses, which also break the symmetry). The characteristic vertex of lepton-flavored dark matter involves contact interactions between χ and the SM leptons of the form shown in the Fig. 2.1. If dark matter couples to the $\mathrm{SU}(2)_W$ doublet leptons L of the SM, the corresponding terms in the Lagrangian

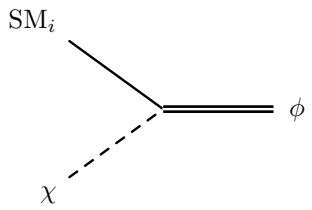

Figure 2.1: Lepton flavored dark matter interaction.

take the schematic form

$$\lambda_A{}^\alpha L^A \chi_\alpha \phi \quad + \text{h.c.}, \tag{2.1}$$

Alternatively, if dark matter couples to the $\mathrm{SU}(2)_W$ singlet leptons E^c, the coupling is given by

$$\lambda_\alpha{}^i \chi^\alpha E_i^c \phi \quad + \text{h.c.} \tag{2.2}$$

Here A is a $\mathrm{U}(3)_L$ flavor index while i is a $\mathrm{U}(3)_E$ flavor index and α is a $\mathrm{U}(3)_\chi$ flavor index. There may also be additional interactions between the dark matter fields and the SM of the form shown in Fig. 2.5, in particular when χ transforms under the $\mathrm{SU}(2)_W$ gauge interactions of the SM.

The particle ϕ that mediates dark matter interactions with the charged leptons is necessarily electrically charged. If χ is a fermion then ϕ must be a boson and vice versa. The same symmetry that makes the dark matter stable ensures that lepton flavor violating processes involving the dark matter field, such as $\mu \to e\gamma$, only arise at loop level through diagrams such as the one shown in Fig. 2.2. For concreteness, in what follows we take χ to be a Dirac fermion and ϕ to be a complex scalar, and restrict our focus to the case where χ couples to the $\mathrm{SU}(2)_W$ singlet lepton field E^c,

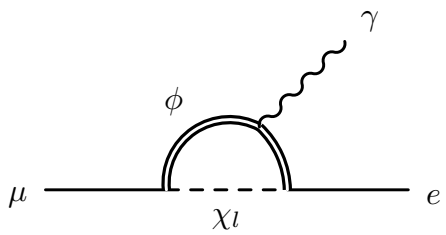

Figure 2.2: Potential contribution to $\mu \to e\gamma$ from lepton flavored dark matter.

as in Eq. 2.2. The generalization to the other cases is straightforward, and is left for future work.

In general the matrix λ will contain both diagonal and off-diagonal elements, thereby giving rise to lepton flavor violation. The experimental bounds on such processes are satisfied if all the elements in the matrix λ are less than 10^{-3} for $m_\phi \sim 200$ GeV, even in the absence of any special flavor structure. In spite of these small couplings such a theory can still lead to interesting collider signals, since ϕ can be pair produced through SM gauge interactions, and will emit charged leptons as it decays down to the dark matter particle. However, couplings of this size are by themselves too small to generate the correct abundance for χ, if it is to be a thermal relic. This is not necessarily a problem if χ transforms under the $\mathrm{SU}(2)_W$ gauge interactions of the SM, or more generally if the theory has additional vertices of the form shown in Fig. 2.5, since these other couplings can play a role in determining the relic abundance. However, if χ is a SM singlet and has no sizable couplings beyond those in Eq. 2.2, the elements in λ must be of order unity to generate the observed amount of dark matter, and aligned with the lepton Yukawa couplings to avoid flavor bounds.

The matrix λ can naturally be aligned with the SM Yukawa couplings if this interaction preserves a larger subgroup of the SM flavor group than just overall lepton number. For example, if we identify the three flavors of dark matter with the electron, muon and tau flavors in the SM, alignment is obtained if λ, and the dark matter mass matrix, respects the $\mathrm{U}(1)^3$ symmetry of lepton sector of the SM. In other words, the $\mathrm{U}(3)_\chi \times \mathrm{U}(3)^2$ symmetry is explicitly broken by λ, and by the SM Yukawa couplings, down to the diagonal $\mathrm{U}(1)^3$. This larger symmetry forbids lepton flavor violating processes.

A more restrictive possibility is that the only source of flavor violation in the theory is the SM Yukawa matrix, which then constrains the coupling matrix λ to be consistent with MFV. In this scenario, the dark matter flavor symmetry $\mathrm{U}(3)_\chi$ is identified with either $\mathrm{U}(3)_E$ or $\mathrm{U}(3)_L$ of the SM, and the matrix λ respects these symmetries up to effects arising from the SM Yukawa couplings.

If we write the lepton Yukawa couplings of the SM as

$$y_A{}^i L^A E_i^c H \quad + \text{h.c.}, \tag{2.3}$$

then the Yukawa matrix $y_A{}^i$ can be thought of as a spurion transforming as $(3, \bar{3})$ under the $\mathrm{SU}(3)_L \times \mathrm{SU}(3)_E$ subgroup of $\mathrm{U}(3)_L \times \mathrm{U}(3)_E$. We now consider the cases where $U(3)_\chi$ is identified with $U(3)_E$ or with $U(3)_L$ separately.

$\mathrm{U}(3)_\chi$ identified with $\mathrm{U}(3)_E$

Consider first the case where $\mathrm{U}(3)_\chi$ is identified with $\mathrm{U}(3)_E$. Then we obtain

$$\lambda_\alpha{}^i \chi^\alpha E_i^c \phi \quad + \text{h.c.} \to \lambda_j{}^i \chi^j E_i^c \phi \quad + \text{h.c.} \tag{2.4}$$

If the theory respects MFV the matrix λ is restricted to be of the form

$$\lambda_j{}^i = \left(\alpha \mathbb{1} + \beta\, y^\dagger y\right)_j{}^i \,. \tag{2.5}$$

Here α and β are constants, and we are keeping only the first non-trivial term in an expansion in powers of the SM Yukawa couplings.

We write the dark matter mass matrix schematically as

$$[m_\chi]_\beta{}^\alpha \bar{\chi}_\alpha \chi^\beta. \tag{2.6}$$

In this case MFV restricts m_χ to have the form

$$[m_\chi]_i{}^j = \left(m_0 \mathbb{1} + \Delta m\, y^\dagger y\right)_i{}^j, \tag{2.7}$$

where m_0 and Δm are constants.

The spectrum and phenomenological implications arising from this scenario depend sensitively on the values of the parameters β and Δm. In any specific model, these constants will depend on details of the underlying ultraviolet physics. However, we expect that in the absence of tuning, any theory where the Yukawa couplings constitute a sufficiently small breaking of the flavor symmetry that the perturbative expansions of the matrices λ and m_χ in powers of the Yukawa couplings, Eqs. 2.5 and 2.7, will satisfy the inequalities

$$\begin{aligned} |\alpha| &\gg |\beta y_\tau^2| \\ |m_0| &\gg |\Delta m y_\tau^2| \,. \end{aligned} \tag{2.8}$$

Here y_τ is the Yukawa coupling of the tau lepton in the SM.

However, it is worth noting that the parameters β and Δm are **not** in general restricted to take values such that the inequalities

$$\begin{aligned} |\alpha| &\gg |\beta| \\ |m_0| &\gg |\Delta m| \end{aligned} \tag{2.9}$$

are satisfied. As a concrete example of a model that violates these inequalities, consider a two Higgs doublet extension of the SM where in the ultraviolet one Higgs doublet couples to the quarks and the other to the leptons. The lepton Yukawa couplings in this theory, though proportional to the corresponding SM Yukawa couplings, can in general be much larger than in the SM. In this scenario, radiative corrections to β and Δm alone can easily be large enough to violate the inequalities in Eq. 2.9 above. Note that this is true even if at the weak scale there is only one light Higgs doublet, which arises as a linear combination of the two present at high energies, the orthogonal combination being heavy.

Since the SM Yukawa couplings of the first two generations are very small, we see that the corresponding dark matter flavors have very small splittings and couple in a flavor diagonal way with approximately equal strength to leptons of the SM. For dark matter masses of order 100 GeV, these mass splittings are less than a GeV. The tau flavored dark matter state can, however, be split from the other two by up to tens of GeV. The strength of its couplings to the SM may also be somewhat different from the other flavors. Either the tau flavored or the electron flavored state will be the lightest, depending on the sign of Δm.

$\mathrm{U}(3)_\chi$ identified with $\mathrm{U}(3)_L$

We now turn to the case where $\mathrm{U}(3)_\chi$ is identified with $\mathrm{U}(3)_L$. Then

$$\lambda_\alpha{}^i \chi^\alpha E_i^c \phi \quad + \text{h.c.} \to \lambda_A{}^i \chi^A E_i^c \phi \quad + \text{h.c.} \tag{2.10}$$

MFV restricts the matrix λ to be of the form

$$\lambda_A{}^i = \alpha \, y_A{}^i \,, \tag{2.11}$$

where again we are working only to the leading non-trivial order in an expansion in the SM Yukawa couplings. The dark matter mass matrix now takes the form

$$[m_\chi]_A{}^B = \left(m_0 \mathbb{1} + \Delta m \; y y^\dagger\right)_A{}^B. \tag{2.12}$$

We see that as in the previous case the electron and muon dark matter flavors are necessarily close in mass, while for large values of Δm the tau flavor can be somewhat split. However, the couplings of the different dark matter flavors to the SM fields, though still flavor-diagonal, are now hierarchical. In particular, if the relic abundance is determined by λ, we expect that only the tau flavor can constitute thermal relic dark matter, since the couplings of the other flavors are relatively small.

2.2 Quark Flavored Dark Matter

Let us now consider the case where dark matter carries quantum numbers under quark flavor. The quark sector of the SM has a $\mathrm{U}(3)_Q \times \mathrm{U}(3)_U \times \mathrm{U}(3)_D$ flavor symmetry, where $\mathrm{U}(3)_Q$ acts on the $\mathrm{SU}(2)_W$ doublet quarks and $\mathrm{U}(3)_U$ and $\mathrm{U}(3)_D$

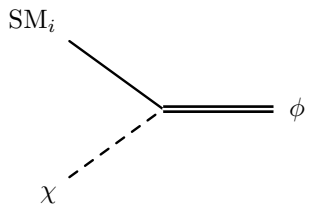

Figure 2.3: Quark flavored dark matter interactions.

on the up and down-type singlet quarks. This symmetry is explicitly broken down to U(1) baryon number by the SM Yukawa couplings.

The characteristic vertex of quark flavored dark matter (QFDM) has the form shown in Fig. 2.3. The corresponding terms in the Lagrangian take the schematic form

$$\lambda_A{}^{\alpha} Q^A \chi_\alpha \, \phi \quad + \text{h.c.} \, , \tag{2.13}$$

if dark matter couples to the $\mathrm{SU}(2)_W$ doublet quarks Q. Alternatively, if it couples to the $\mathrm{SU}(2)_W$ singlet up-type quarks U^c, we have

$$\lambda_\alpha{}^{i} \chi^\alpha U_i^c \, \phi \quad + \text{h.c.} \tag{2.14}$$

This is easily generalized to the case where dark matter transforms under $\mathrm{U}(3)_D$,

$$\lambda_\alpha{}^{a} \chi^\alpha D_a^c \, \phi \quad + \text{h.c.} \tag{2.15}$$

Here the index A represents a $\mathrm{U}(3)_Q$ flavor index while i is a $\mathrm{U}(3)_U$ flavor index and a is a $\mathrm{U}(3)_D$ flavor index. The mediator ϕ is now charged under both color and electromagnetism. For concreteness, in what follows we again take χ to be a Dirac fermion and ϕ to be a complex scalar, and restrict our focus to the cases where χ

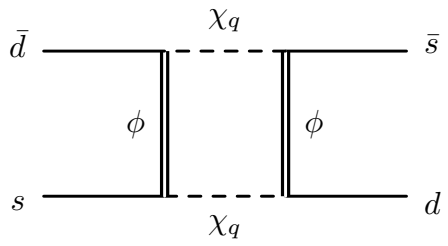

Figure 2.4: Potential contribution to $K - \bar{K}$ mixing from quark flavored dark matter.

couples to the $\mathrm{SU}(2)_W$ singlet quarks U^c or D^c as in Eq. 2.14 and Eq. 2.15. The generalization to other cases is straightforward, and is left for future work.

Contributions to flavor violating processes, such as $K - \bar{K}$ mixing, arise at loop level through diagrams such as the one in Fig. 2.4. The experimental bounds on flavor violation are satisfied if all the elements in $\lambda \lesssim 10^{-2}$, for $m_\phi \sim 500$ GeV. However, as in the lepton case, couplings of this size are by themselves too small to generate the correct abundance for χ, if it is to be a thermal relic. This is not necessarily a problem if χ has additional interactions with the SM, since these may set the relic abundance. However, if χ is a SM singlet and has no other sizable couplings, the elements in λ must be of order unity to generate the observed amount of dark matter. In this case the interaction matrix λ must be aligned with the SM Yukawa couplings if the flavor constraints are to be satisfied.

For the matrix λ to be naturally aligned with the SM Yukawa couplings this interaction must preserve, at least approximately, a larger subgroup of the SM flavor group than just baryon number. This constraint is satisfied if the couplings λ are consistent with MFV. In this framework, the only sources of flavor violation are the

SM Yukawa couplings, and the matrix λ respects the SM flavor symmetries up to effects that arise from them.

2.2.1 Coupling with up-type Quarks

Consider first the case when dark matter couples to the up-type $\mathrm{SU}(2)_W$ singlet quarks U^c as in Eq. 2.14. MFV can be realized if the dark matter flavor symmetry $\mathrm{U}(3)_\chi$ is identified with one of $\mathrm{U}(3)_U$, $\mathrm{U}(3)_Q$ or $\mathrm{U}(3)_D$ of the SM, and the matrix λ respects these symmetries up to effects arising from the SM Yukawa couplings. As in the lepton case, we will work to the leading non-trivial order in an expansion in powers of the SM Yukawa couplings.

The quark Yukawa couplings in the SM can be written as

$$\hat{y}_A{}^a Q^A D^c_a H + y_A{}^i Q^A U^c_i H^\dagger \quad + \text{h.c.} \tag{2.16}$$

The up-type Yukawa matrix y can be thought of as a spurion transforming as $(3, \bar{3}, 1)$ under the $\mathrm{SU}(3)_Q \times \mathrm{SU}(3)_U \times \mathrm{SU}(3)_D$ subgroup of $\mathrm{U}(3)_Q \times \mathrm{U}(3)_U \times \mathrm{U}(3)_D$, while the down-type matrix $\hat{y}$ can be thought of as a spurion transforming as $(3, 1, \bar{3})$.

We now look at each of the cases in detail where $U(3)_\chi$ is identified with $U(3)_Q$, $U(3)_U$ and $U(3)_D$.

$\mathrm{U}(3)_\chi$ identified with $\mathrm{U}(3)_U$

If $\mathrm{U}(3)_\chi$ is identified with $\mathrm{U}(3)_U$, MFV restricts the matrix λ to be of the form

$$\lambda_i{}^j = \left(\alpha \mathbb{1} + \beta\, y^\dagger y\right)_i{}^j \,, \tag{2.17}$$

while the mass matrix for χ becomes

$$[m_\chi]_i^j = \left(m_0 \mathbb{1} + \Delta m \; y^\dagger y\right)_i^{\;j}. \tag{2.18}$$

As explained earlier, we are working to leading non-trivial order in an expansion in powers of the SM Yukawa couplings. We expect that in any theory where the Yukawa couplings constitute a sufficiently small breaking of the flavor symmetry that such expansions of λ and m_χ in powers of the Yukawa couplings are permitted, in the absence of tuning the inequalities

$$\begin{aligned} \alpha &\gtrsim \beta y_t^2 \\ m_0 &\gtrsim \Delta m y_t^2 \, , \end{aligned} \tag{2.19}$$

will be satisfied. Here y_t is the Yukawa coupling of the top in the SM. The effect of these inequalities is to constrain the mass splittings between the different dark matter flavors, and to restrict the extent to which their couplings can differ.

It follows from this discussion that the dark matter states that couple to the first two generations of SM quarks are nearly degenerate in mass, and the mixing between them and the state with top flavor is small, protecting against flavor violating processes. For a dark matter mass of 100 GeV, the splitting between the up and charm flavored dark matter states is less than 10 MeV. The splitting between these states and the top flavored state can however be significantly larger, as much as tens of GeV. The physical dark matter particle is expected to be either up flavored or top flavored, depending on the sign of Δm.

$U(3)_\chi$ identified with $U(3)_Q$

If $U(3)_\chi$ is identified with $U(3)_Q$ we have instead

$$\lambda_A{}^i = \kappa\, y_A{}^i. \tag{2.20}$$

The dark matter mass matrix now takes the form

$$[m_\chi]_A{}^B = \left(m_0 \mathbb{1} + \Delta m\, yy^\dagger + \hat{\Delta} m\, \hat{y}\hat{y}^\dagger\right)_A{}^B. \tag{2.21}$$

The consistency of our expansion in powers of the Yukawa couplings requires that the inequalities $m_0 \gtrsim \hat{\Delta} m y_b^2$ and $m_0 \gtrsim \Delta m y_t^2$ be satisfied. Here y_b is the bottom Yukawa coupling in the SM. While the first two flavors of χ are again quasi-degenerate in mass, their couplings to the SM are now hierarchical rather than universal. For a dark matter mass of 100 GeV, the dark matter flavors associated with the first two generations are split by less than or of order 100 MeV. The third generation dark matter particle could, however, be split from the others by tens of GeV. It is the smallness of the SM Yukawa couplings of the first two generations and their small mixing with the third generation that protects against flavor changing processes. If the splittings between the third generation dark matter particle and the other two flavors is much larger than the temperature at freeze out, we expect that the observed dark matter will belong to the third generation, since the other flavors couple too weakly to give rise to the observed relic abundance.

$U(3)_\chi$ identified with $U(3)_D$

Finally, if $U(3)_\chi$ is identified with $U(3)_D$, we have

$$\lambda_a{}^i = \hat{\kappa} \left(\hat{y}^\dagger y\right)_a{}^i \tag{2.22}$$

and

$$[m_\chi]_a{}^b = \left(m_0 \mathbb{1} + \Delta m \; \hat{y}^\dagger \hat{y}\right)_a{}^b \, . \tag{2.23}$$

For consistency we require $m_0 \gtrsim \Delta m y_b^2$. Once again the first two flavors are very close in mass, and their couplings to the SM hierarchical. For a dark matter mass of order 100 GeV their splitting is expected to be less than or of order 100 MeV. The mass of the bottom flavored dark matter state can be split from the other two flavors by tens of GeV. If the splittings between the bottom flavored state and the others are much larger than the temperature at freeze out, the lightest particle must be bottom flavored to generate the observed abundance of dark matter.

2.2.2 Coupling with down-type Quarks

We now turn our attention to the case where dark matter couples to the $SU(2)_W$ singlet down-type quarks D^c as in Eq. 2.15. MFV can be realized if the dark matter flavor symmetry $U(3)_\chi$ is identified with one of $U(3)_D$, $U(3)_Q$ or $U(3)_U$ of the SM. The corresponding formulas for the form of the coupling matrix λ and the dark matter mass may be obtained by simply interchanging y and $\hat{y}$ in the equations above.

$\mathrm{U}(3)_\chi$ identified with $\mathrm{U}(3)_D$

If $\mathrm{U}(3)_\chi$ is identified with $\mathrm{U}(3)_D$, the matrix λ is constrained to be of the form

$$\lambda_a{}^b = \left(\alpha \mathbb{1} + \beta\ \hat{y}^\dagger \hat{y}\right)_a{}^b , \tag{2.24}$$

while the dark matter mass matrix is now

$$[m_\chi]_a{}^b = \left(m_0 \mathbb{1} + \hat{\Delta} m\ \hat{y}^\dagger \hat{y}\right)_a{}^b . \tag{2.25}$$

Rather than Eq. 2.19, we now have

$$\begin{aligned} \alpha &\gtrsim \beta y_b^2 \\ m_0 &\gtrsim \hat{\Delta} m y_b^2 \, . \end{aligned} \tag{2.26}$$

We see that the states associated with the first two generations are quasi-degenerate in mass and couple universally to the SM, while the third generation can be somewhat split. This fact, together with the small mixing between the third flavor of dark matter and the first two allows flavor constraints to be satisfied. We expect that either the bottom or down flavor will constitute dark matter.

$\mathrm{U}(3)_\chi$ identified with $\mathrm{U}(3)_Q$

If $\mathrm{U}(3)_\chi$ is instead identified with $\mathrm{U}(3)_Q$, we have

$$\lambda_A{}^a = \kappa\ \hat{y}_A{}^a , \tag{2.27}$$

while the mass matrix is of the form

$$[m_\chi]_A{}^B = \left(m_0 \mathbb{1} + \Delta m\ y y^\dagger + \hat{\Delta} m\ \hat{y} \hat{y}^\dagger\right)_A{}^B . \tag{2.28}$$

We expect that the parameters will satisfy the inequalities $m_0 \gtrsim \Delta m y_t^2$ and $m_0 \gtrsim \hat{\Delta} m y_b^2$. While the first two generations are still nearly degenerate, the different flavors now couple to the SM hierarchically rather than universally. As a consequence we expect that if dark matter is a thermal relic, and the splitting between the different flavors of χ is much larger than the temperature at freeze out, the observed dark matter will be composed of third generation particles.

$\mathrm{U}(3)_\chi$ identified with $\mathrm{U}(3)_U$

Finally, if $\mathrm{U}(3)_\chi$ is identified with $\mathrm{U}(3)_U$ these formulae become

$$\lambda_i{}^a = \alpha \left(y^\dagger \hat{y}\right)_i{}^a \tag{2.29}$$

and

$$[m_\chi]_i^{\ j} = \left(m_0 \mathbb{1} + \Delta m \; y^\dagger y\right)_i{}^j \, . \tag{2.30}$$

The parameters must satisfy the inequality $m_0 \gtrsim \Delta m y_t^2$. Once again the dark matter states associated with the first two generations are very close in mass, and their couplings to the SM hierarchical. If the splitting between the top flavored state and the other two states is much larger than the temperature at freeze out, the observed dark matter must be top flavored.

2.3 Dark matter with Internal Flavor

Finally we consider the possibility that dark matter carries a new internal flavor quantum number that is distinct from either quark or lepton flavor, and does not

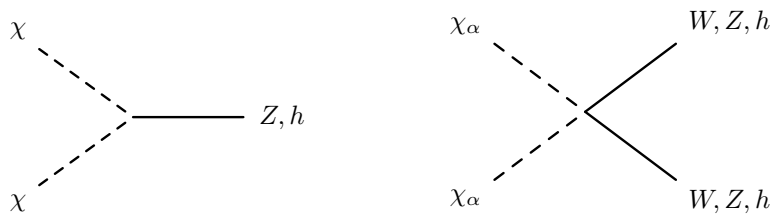

Figure 2.5: Interactions of dark matter with internal flavor

couple directly to the SM matter fields at the renormalizable level. In this framework, the only possible direct interactions of χ with the SM fields at the renormalizable level are to the weak gauge bosons or to the Higgs as shown in Fig. 2.5. These interactions do not generate large new sources of quark or lepton flavor violation. The direct detection signals are very similar to those of the corresponding theory where dark matter does not carry flavor.

These theories are closely related to those where new particles, such as a scalar boson ϕ or vector boson Z', that have couplings of exactly the same form as in Fig. 2.5, mediate interactions between the SM matter fields and the dark matter sector. One important difference is that these can potentially give rise to SM flavor violating effects, if their couplings to the SM fields are off-diagonal.

In this scenario, the dark matter states corresponding to different flavors may be exactly degenerate, if the internal flavor symmetry is exact, or split, if the symmetry is broken. The collider phenomenology is highly sensitive to both the splitting between states, and to the particles produced when heavier states decay to lighter ones. The heavier particles in the dark matter multiplet can be pair produced through their couplings to the Z, the Higgs, ϕ or Z', and can then decay down

to the lightest state. The additional particles produced in these decays, if visible, together with missing energy, constitute the collider signatures. This is a natural framework for a hidden valley [83] where particles such as ϕ or Z' are the portal to the hidden sector. In this scenario, decays may be slow on collider time scales, giving rise to displaced vertices, since the couplings involved can be small in a technically natural way.

The phenomenology of these models is highly sensitive to various model assumptions, and we leave a more detailed analysis of this case to future work.

Chapter 3

Relic Abundance

In this chapter we study the phenomenology of various flavored dark matter models in terms of their thermal relic abundance. In a few cases, the calculation follows the standard relic abundance calculation. However, the specific flavor structure of certain models gives rise to distinct phenomenology.

As before, we will focus on the case where χ is a SM singlet. In general, the dark matter particle could also carry $SU(2)_W$ quantum numbers, which imply additional interactions and affect the relic abundance calculation. We leave this possibility for future work.

3.1 Standard Calculation of Relic Abundance

In this section we derive the relic abundance of a single species which freezes out when it is non-relativistic in more detail. This analysis will justify the formulae and approximations used in Chapter 1.

The relic abundance is determined by solving the Boltzmann equation for the dark matter number density n at late times,

$$\frac{dn}{dt} + 3Hn = -\langle \sigma v \rangle \left(n^2 - n_{eq}^2 \right) \ . \tag{3.1}$$

Here H is the Hubble constant and n_{eq} is the equilibrium number density of χ. The second term accounts for the expansion of the universe. We can recast the equation

in terms of co-moving density of dark matter,

$$\bar{n} = na^3(t) \tag{3.2}$$

so that the Boltzmann equation becomes,

$$\frac{1}{\bar{n}_{eq}}\frac{d\bar{n}}{dt} = -\langle\sigma v\rangle n_{eq}\left[\left(\frac{\bar{n}}{\bar{n}_{eq}}\right)^2 - 1\right] , \tag{3.3}$$

where n_{eq} is the equilibrium dark matter density at a given temperature.

It is convenient to change the independent variable from time t to temperature $x = m_\chi/T$. The dark matter freeze out occurs in radiation dominated epoch, so the time temperature relation is,

$$t = \frac{1}{2H} = \frac{x^2}{2H(m_\chi)}. \tag{3.4}$$

The Boltzmann equation becomes,

$$\frac{x}{\bar{n}_{eq}}\frac{d\bar{n}}{dx} = -\frac{\langle\sigma v\rangle n_{eq}}{H}\left[\left(\frac{\bar{n}}{\bar{n}_{eq}}\right)^2 - 1\right] . \tag{3.5}$$

In this form, it is clear that the evolution of the number density depends critically on the ratio of the annihilation rate to the Hubble parameter,

$$\frac{\Gamma_A}{H} = \frac{\langle\sigma v\rangle n_{eq}}{H}. \tag{3.6}$$

When the rate of annihilation is much faster than the expansion of the universe ($\propto H$), $\bar{n}$ tracks its equilibrium value. As the universe cools, the rate of expansion becomes comparable to the annihilation rate (since the equilibrium number density of dark matter falls exponentially). Upon further cooling, the expansion rate dominates the annihilation rate, and the dark matter density departs from its equilibrium value and freezes out.

The Boltzmann equation does not have an analytical solution, but can be easily solved numerically. We first solve for the relic abundance approximately in order to recover the result in Chapter 1 and then compare it with the numerical result.

The dark matter freezes out at a temperature where its rate of annihilation becomes equal to the expansion rate,

$$\langle \sigma v \rangle \, n_{eq} = H. \tag{3.7}$$

The dark matter freeze out occurs in a radiation dominated era, so the Hubble parameter is given by,

$$H = 1.67 g_*^{1/2} \frac{T^2}{m_{pl}}. \tag{3.8}$$

where $g_* \sim 100$ is the effective number of relativistic degrees of freedom in the SM when the temperature of the universe $T \sim 10$ GeV. The equilibrium density of dark matter is well approximated by the Maxwell-Boltzmann distribution when it is non-relativistic,

$$n_{eq} = g \left(\frac{m_\chi T}{2\pi} \right)^{3/2} \exp[-m_\chi / T], \tag{3.9}$$

where g is the number of degrees of freedom of χ. The freeze out temperature x_f is then the solution of the equation,

$$x_f \; e^{-x_f} = \frac{1.67 g_*^{1/2} (2\pi)^{3/2}}{g \; m_{pl} \, m_\chi \langle \sigma v \rangle}, \tag{3.10}$$

where $x_f = m_\chi / T_f$. The freeze out temperature thus only depends logarithmically on the annihilation cross section, mass and spin of dark matter. For typical weak scale values, $x_f \sim 20$.

The entropy in a co-moving volume is constant under all forms of adiabatic evolution, barring entropy production from a first-order phase transition or out-of-equilibrium decay. In fact, entropy production in these processes is small, and adiabatic evolution is a good approximation to the evolution of our universe. Therefore, the entropy density s serves as an excellent fiducial volume, $\bar{n}_\chi \propto n_\chi/s$, and we can use n_χ/s as a measure of co-moving dark matter density.

The dark matter contribution to the energy density today is given by

$$\Omega_{DM} = \frac{m_\chi n_\chi(x_0)}{\rho_c(x_0)} = m_\chi \frac{1}{\langle\sigma v\rangle}\left[1.67 g_*(x_f)^{1/2}\frac{T_f^2}{m_{pl}}\right]\ \frac{g_{*S}(x_0)T_0^3}{g_{*s}(x_f)T_f^3}\ \frac{1}{3H(x_0)^2 m_{pl}^2} \tag{3.11}$$

$$= x_f \frac{1}{\langle\sigma v\rangle}\left[1.67 g_*(x_f)^{1/2}\frac{1}{m_{pl}}\right]\ \frac{g_{*S}(x_0)T_0^3}{g_{*s}(x_f)}\ \frac{1}{3H(x_0)^2 m_{pl}^2}, \tag{3.12}$$

where g_{*s} is the effective number of relativistic degrees of freedom such that the entropy density $s \sim g_{*S}T^3$, and the relic dark matter number density was taken to be the equilibrium number density at the freeze out temperature x_f.

This approximation compares well to the numerical solution of Boltzmann equations plotted in Fig. 3.1.

As noted in Chapter 1, the relic abundance of dark matter dominantly depends on the annihilation cross section. The dependence on spin and mass of the dark matter is through the freeze out temperature x_f, and hence logarithmic. The correct dark matter density ($\Omega_{DM} \simeq 0.23$) is obtained when the annihilation cross section is weak scale,

$$\langle\sigma v\rangle \simeq 3 \times 10^{-26}\ \mathrm{cm}^3/\mathrm{s}. \tag{3.13}$$

In the subsequent sections we analyze the extent to which the standard analysis

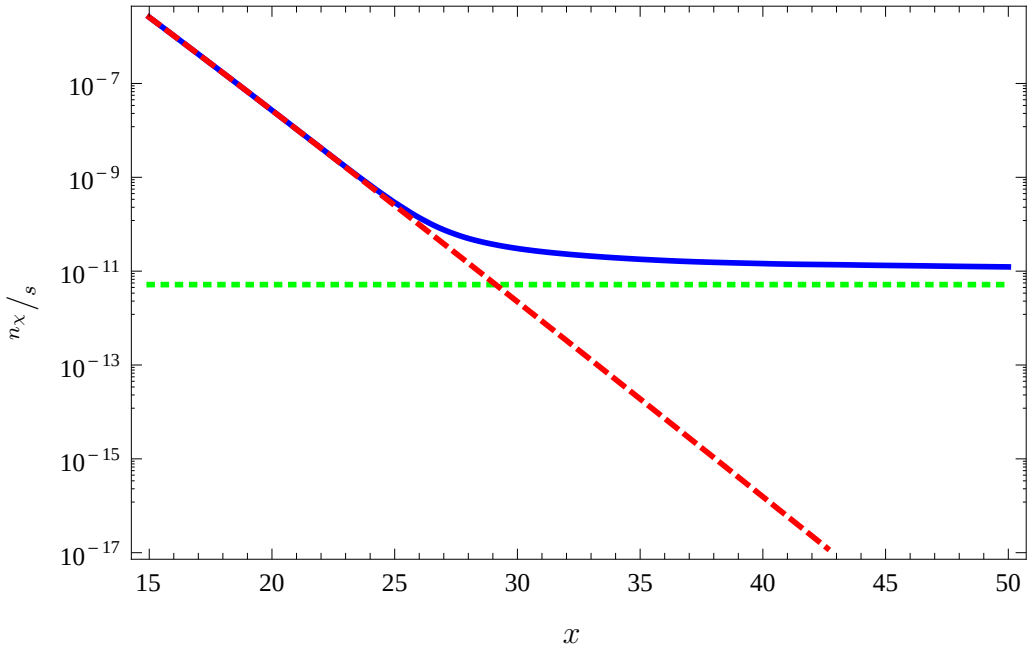

Figure 3.1: Freeze out of a single species of dark matter with annihilation cross section $\langle \sigma v \rangle = 3 \times 10^{-26}$ cm^3/s. The solid blue curve shows the dark matter density normalized to the entropy density n_χ/s, the dashed red curve shows the equilibrium thermal density of dark matter and the dotted green curve shows the equilibrium density at freeze out ($x = x_f$) as defined in the text.

of WIMP freeze out is modified in FDM due to the potential presence of multiple species of dark matter in thermal equilibrium at freeze out.

3.2 Lepton Flavored Dark Matter

We will concentrate on the case where χ is a SM singlet, its only interactions are those of Eq. 3.14,

$$\lambda_\alpha{}^i \chi^\alpha E_i^c \phi \quad + \text{h.c.} \tag{3.14}$$

The primary annihilation mode is through t-channel ϕ exchange to two leptons. In the relevant parameter space, the matrix λ is constrained by flavor bounds to be very nearly flavor diagonal, so each state in the dark matter multiplet is associated with a specific lepton flavor.

The relevant terms in the Lagrangian, written schematically in 4-component Dirac notation, take the form

$$\mathcal{L} \supset \frac{\lambda}{2} \left[\bar{\chi}(1+\gamma_5)\ell \, \phi + \bar{\ell}(1-\gamma_5)\chi \, \phi^\dagger \right] \ . \tag{3.15}$$

Here χ represents the physical dark matter state and l the corresponding lepton. We have suppressed flavor indices since the matrix λ is constrained to be nearly diagonal in the relevant region of parameter space. Since the dark matter particle is non-relativistic at freeze-out, annihilation is dominated by the lowest partial wave. In this limit

$$\langle \sigma v \rangle = \frac{\lambda^4 m_\chi^2}{32\pi (m_\chi^2 + m_\phi^2)^2} \ , \tag{3.16}$$

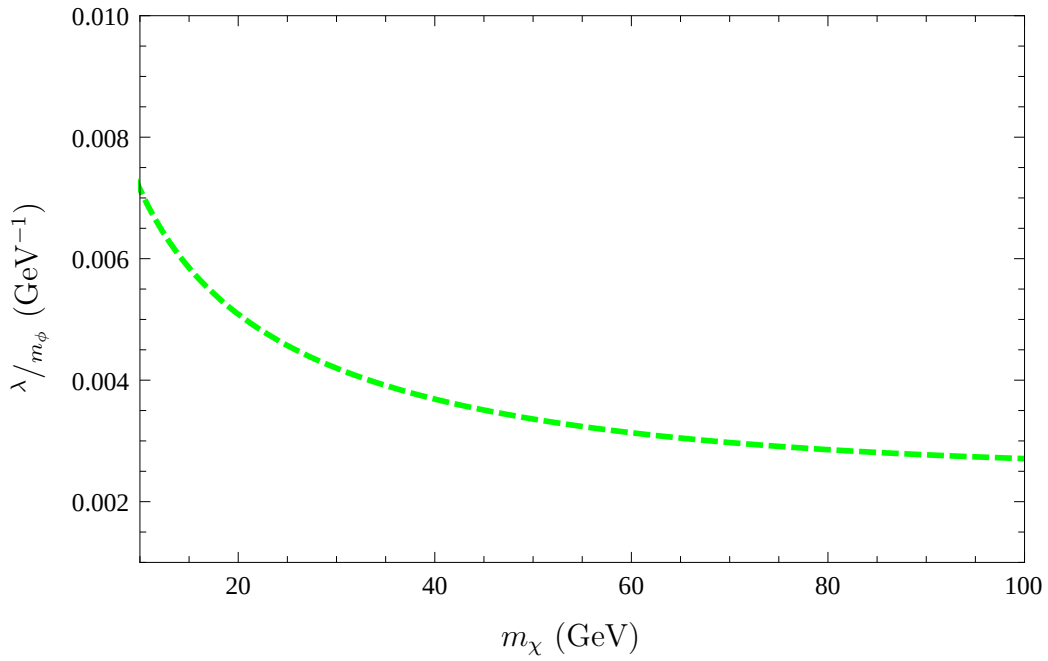

Figure 3.2: Relic abundance constraints on τ-lepton flavored dark matter when $m_\phi = 150$ GeV.

where we have assumed that $m_\chi \gg m_\ell$, so that the masses of the final state leptons can be neglected.

If the splittings between the different states in this multiplet are large enough that the heavier states do not play a significant role in determining the relic abundance of the lightest state, the standard relic abundance calculation performed in the previous section applies.

In the limit that $m_\phi \gg m_\chi$, the constraint that the relic abundance agree with observation determines λ/m_ϕ as a function of the dark matter mass. As an example, we plot the coupling as a function of dark matter mass for τFDM model in Fig. 3.2.

3.2.1 Degenerate Flavors with Universal Couplings

If the splitting between the different flavors of dark matter is sufficiently small, more than one dark matter species may be present at freeze out. In this case co-annihilations play a significant role, and must be taken into account in the relic abundance calculation. For concreteness, we focus on the MFV scenarios considered in the previous section. We first consider the case where dark matter transforms under $\mathrm{U}(3)_E$, and where the splittings are such that the electron and muon flavors of dark matter are both present during freeze out, but not the tau flavor. Depending on the splittings, the muon flavored state may either subsequently decay to the electron flavored state, or remain stable on cosmological time scales so as to constitute a component of the observed dark matter. In either case the number density of dark matter is unaffected.

In this framework, the cross sections for $\chi_e\chi_\mu$ and $\chi_\mu\chi_\mu$ annihilations are both equal to that for $\chi_e\chi_e$ annihilation, given by Eq. 3.16. If the mass splitting between the two species is much smaller than the temperature at freeze out, n_{eq} is also the same for both species. If we denote the number density of electron flavored dark matter by n_e, and that of the muon flavor by n_μ, the Boltzmann equations take the form

$$\begin{aligned}
\frac{dn_e}{dt} + 3Hn_e &= -\langle\sigma v\rangle \left[\left(n_e^2 - n_{eq}^2\right) + \left(n_e n_\mu - n_{eq}^2\right)\right] \\
&\quad - \left[\chi_e \to \chi_\mu\right] \\
\frac{dn_\mu}{dt} + 3Hn_\mu &= -\langle\sigma v\rangle \left[\left(n_\mu^2 - n_{eq}^2\right) + \left(n_e n_\mu - n_{eq}^2\right)\right] \\
&\quad - \left[\chi_\mu \to \chi_e\right] \ . \qquad (3.17)
\end{aligned}$$

Here $\chi_e \to \chi_\mu$ denotes the net effect of scattering processes such as $e\chi_e \leftrightarrow \mu\chi_\mu$ as well as decays and inverse decays which convert the electron flavor of dark matter into the muon flavor and vice versa, but leave the overall dark matter density $N = n_e + n_\mu$ unaffected. Recognizing that the relic abundance is set by the value of N at late times, we can combine the equations above to obtain a single equation for N,

$$\frac{dN}{dt} + 3HN = -\langle\sigma v\rangle \left(N^2 - 4n_{eq}^2\right) \ . \tag{3.18}$$

This equation has a very similar form to the Boltzmann equation for a single dark matter species, and can be solved in exactly the same way. We find that the relic abundance is in fact relatively insensitive to the change in the number of dark matter species, changing by only about 5% when other parameters are kept fixed. A very similar analysis shows that the same conclusion holds true when the splittings are small enough that the tau flavor of dark matter is also in the bath at freeze out. It follows that the results from the single flavor case, Eq. 3.16, also apply to the cases of more than one dark matter flavor, up to fairly small corrections.

3.2.2 Degenerate Flavors with Hierarchical Couplings

We now move on to the case where dark matter transforms under $\mathrm{U}(3)_L$, and all three flavors are present at freeze out. For simplicity we work in the limit where the splitting between all the different flavors is much smaller than the temperature at freeze out, and can be neglected. Since the couplings of the different dark matter flavors to the corresponding SM fermions are now hierarchical, the cross section for $\chi_\tau\chi_\tau$ annihilation is larger by more than two orders of magnitude than that for

$\chi_\tau\chi_\mu$ annihilation, which can be neglected. The cross sections for $\chi_\mu\chi_\mu$, $\chi_\tau\chi_e$, $\chi_\mu\chi_e$ and $\chi_e\chi_e$ are even smaller, and these processes can also be neglected. The relevant Boltzmann equations then take the form

$$\begin{aligned}
\frac{dn_e}{dt} + 3Hn_e &= -\left[\chi_e \to \chi_\mu, \chi_\tau\right] \\
\frac{dn_\mu}{dt} + 3Hn_\mu &= -\left[\chi_\mu \to \chi_e, \chi_\tau\right] \\
\frac{dn_\tau}{dt} + 3Hn_\tau &= -\langle\sigma v\rangle \left[\left(n_\tau^2 - n_{eq}^2\right)\right] - \left[\chi_\tau \to \chi_{\mu,e}\right] \ .
\end{aligned} \tag{3.19}$$

The relic abundance of dark matter depends on whether processes which change the flavor of dark matter but conserve total dark matter number, such as $e\chi_e \leftrightarrow \tau\chi_\tau$, $\mu\chi_\mu \leftrightarrow \tau\chi_\tau$ etc. remain in equilibrium during the freeze out process. If this is the case then the relative fractions n_e/n_τ and n_μ/n_τ closely track their equilibrium value ~ 1. Then we can add these equations to obtain a single equation for the total dark matter number $N = n_e + n_\mu + n_\tau$,

$$\frac{dN}{dt} + 3HN = -\langle\sigma v\rangle \left(\frac{N^2}{9} - n_{eq}^2\right) \ . \tag{3.20}$$

This equation has a very similar form to that of the Boltzmann equation for a single species, but for the factor of 9, which is the square of the number of dark matter flavors. To generate the observed dark matter density then requires the annihilation cross section to be a factor of 9 larger than in the single flavor case. This implies that the correct relic abundance is obtained if λ for the τ flavor is a factor of $\sqrt{3}$ larger than in the single flavor case, Eq. 3.16. If, however, the processes which change dark matter flavor $e\chi_e \leftrightarrow \tau\chi_\tau$ and $\mu\chi_\mu \leftrightarrow \tau\chi_\tau$ go out of equilibrium much before χ_τ freezes out, the surviving χ_μ and χ_e will contribute too much to the dark matter density to be consistent with observations.

In general, for realistic values of the parameters, the process $\mu\chi_\mu \leftrightarrow \tau\chi_\tau$ will be in equilibrium during freeze out. However, the rate for $e\chi_e \leftrightarrow \tau\chi_\tau$, which, though enhanced by a Boltzmann factor, is suppressed by the ratio m_e^2/m_τ^2 relative to the annihilation process $\chi_\tau\chi_\tau \to \tau\tau$, is generally of order the expansion rate at freeze out. Therefore the approximation $n_e/n_\tau = 1$ may not be valid, and cannot be used to simplify the coupled equations (3.19). A preliminary numerical study nevertheless suggests that if λ for the τ flavor is larger than in the single flavor case by a factor close to $\sqrt{3}$, the correct abundance of dark matter is indeed obtained. However, we leave a detailed analysis of this scenario for future work.

If χ is also charged under the SM $\mathrm{SU}(2)_W$ gauge interactions then new annihilation channels open up. Dark matter can annihilate into two W's, two Z's, and also into SM fermions through through s-channel Z exchange. We leave a study of this for future work.

3.3 Quark Flavored Dark Matter

If the primary interaction of dark matter with the SM is through the following couplings,

$$\lambda_\alpha{}^i \chi^\alpha U_i^c \, \phi \;\; + \text{h.c.} \qquad \text{or} \qquad \lambda_\alpha{}^a \chi^\alpha D_a^c \, \phi \;\; + \text{h.c.} \tag{3.21}$$

then the relic abundance is set by t-channel annihilation to quarks. The calculation in this case mirrors that of the lepton flavored dark matter. In cases where the dominant annihilation mode is kinematically forbidden (e.g. for the top quark), three-body final states or loop-suppressed processes may dominate.

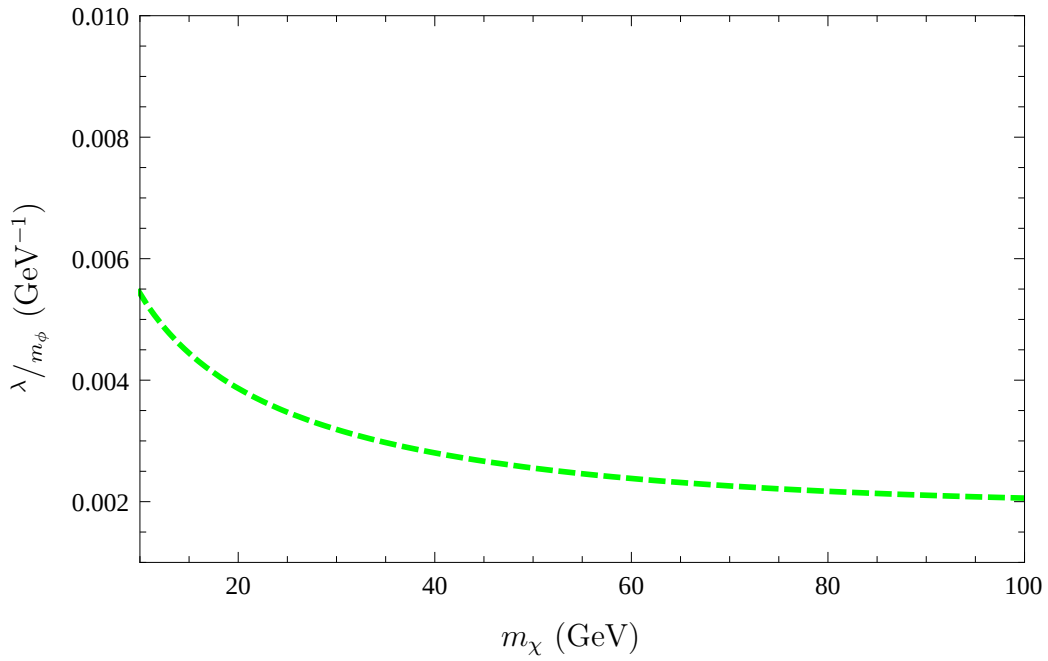

Figure 3.3: Relic abundance constraints on b-quark flavored dark matter when $m_\phi = 150$ GeV.

In the region of parameter space which gives rise to the observed relic abundance, constraints on flavor changing neutral current processes require that the interaction matrix λ be closely aligned with the quark Yukawa couplings. We therefore limit our analysis to the case where λ is consistent with MFV. Then, in the mass basis each particle in the dark matter multiplet is associated with the flavor of the quark it couples to most strongly, and does not mix significantly with the other flavors. We begin by considering the case when the splittings between the particles in the dark matter multiplet are large enough that only the lightest state is present in the bath on the time scales when freeze out occurs. We will relax this assumption later. The relevant terms in the Lagrangian, written in Dirac 4-component notation,

take the schematic form

$$\mathcal{L} \supset \frac{\lambda}{2}\left[\bar{\chi}(1+\gamma_5)q\ \phi + \bar{q}(1-\gamma_5)\chi\ \phi^\dagger\right]\ . \tag{3.22}$$

Here χ represents the physical dark matter particle and q the corresponding quark. MFV ensures that the coupling matrix λ is flavor diagonal in the quark mass basis, allowing us to suppress flavor indices. In the limit that the masses of the final state quarks can be neglected, we find for the annihilation rate

$$\langle \sigma v \rangle = \frac{3\lambda^4 m_\chi^2}{32\pi(m_\chi^2 + m_\phi^2)^2}\ . \tag{3.23}$$

The additional factor of 3 relative to the lepton case arises because of the three colors of quarks. The relic abundance can then be determined from the Boltzmann equation, and λ/m_ϕ determined as a function of the dark matter mass (Fig. 3.3).

3.3.1 Degenerate Flavors

The splitting between the different dark matter flavors may be small enough that more than one species is present in the bath during freeze out. In particular, it follows from our MFV analysis that if the lightest dark matter particle carries either the up or down flavor, the splitting between it and the nearest state is expected to be small enough that both species are present in the bath during freeze out. For some range of parameters, the splittings are such that all three flavors are present. In such a scenario, co-annihilations are expected to play a significant role, and will affect the relic abundance of dark matter.

For concreteness, we focus on the realizations of MFV where dark matter couples to the down-type $\mathrm{SU}(2)_W$ singlet quarks D^c as in Eq. 2.15. We first consider

the case where χ transforms under $\mathrm{U}(3)_D$ and the lightest state carries down flavor. The splittings are assumed to be such that both the down and strange flavored states are in the bath at freeze out. In this realization of MFV, the different flavors of dark matter couple with equal strength to the associated SM particles, and so the cross sections for $\chi_d\chi_s$ and $\chi_s\chi_s$ annihilation are equal to that for $\chi_d\chi_d$ annihilation. Then an analysis very similar to that in the lepton case shows that if all other parameters are kept fixed, the presence of the extra quasi-degenerate species only alters the relic abundance by about 5%. Therefore the parameters that generate the correct relic abundance in the case of quasi-degenerate dark matter flavors differ only slightly from the corresponding parameters in the non-degenerate case. The same conclusion holds if the bottom flavored state is also in the bath at freeze out.

We move on to the scenario where χ transforms under $\mathrm{U}(3)_Q$. In this case the couplings of χ are hierarchical, and so if the lightest state is associated with the first generation, it must be quasi-degenerate with the others to obtain the correct relic abundance. For concreteness we focus on the case where the splittings are negligible compared to the freeze out temperature. Then for realistic values of the parameters the processes $d\chi_d \leftrightarrow b\chi_b$ and $s\chi_s \leftrightarrow b\chi_b$, which convert one flavor of dark matter into another, are in equilibrium at freeze out. Then an analysis identical to that in the leptonic case shows that the correct relic abundance is obtained if the coupling λ for the third generation is larger by a factor of $\sqrt{3}$ than in the single flavor case.

Chapter 4

Direct Detection

Dark matter particles in the galactic halo can scatter off matter particles on Earth. Direct detection experiments seek to detect the energy deposition of nuclear recoil resulting from these interactions.

Flavored dark matter models have unique implications for direct detection experiments and have rich phenomenology depending upon the specifics of the model. We study various cases in detail below.

4.1 Lepton Flavored Dark Matter

Lepton flavored dark matter does not have renormalizable contact interactions with quarks. Although in theories of electron flavored dark matter, χ can scatter off electrons at tree level, the energy transfer is generally not enough to generate a signal in these experiments [84]. Therefore we focus on nuclear recoils.

The direct detection signals of this class of theories depend on whether the dark matter particle χ transforms non-trivially under the SM $SU(2)_W$ gauge symmetry, or remains a SM singlet. If χ is a SM singlet, the leading contribution to dark matter scattering off a nucleus arises from the loop diagrams involving leptons shown in Fig. 4.1.

In the region of parameter space of interest to current direct detection experi-

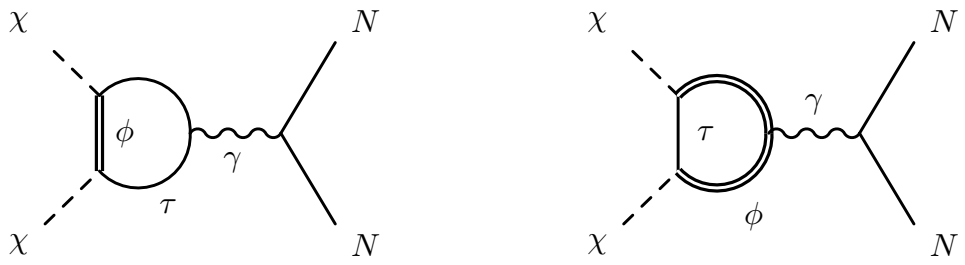

Figure 4.1: Dark matter scattering off a nucleus through photon exchange.

ments, bounds on lepton flavor violating processes constrain the coupling matrix λ to be flavor diagonal. In this case the dark matter candidate carries the flavor of the lepton it couples to. We first consider the case where the splittings between the different dark matter flavors is large, so that a single flavor constitutes all the observed dark matter. We will relax this assumption later. In this limit the relevant terms in the Lagrangian are again those shown in Eq. 3.15. As explained in Appendix A, this coupling gives rise to three distinct types of interactions between dark matter and the nucleus, specifically a charge-charge, a dipole-charge, and a dipole-dipole interaction.

The differential cross section for the charge-charge interaction is given by the expression,

$$\frac{d\sigma_{ZZ}}{dE_r} = \frac{2m_{nuc}}{4\pi v^2} Z^2 \, b_p^2 \, F^2(E_r) \ , \tag{4.1}$$

where m_{nuc} is the mass of the nucleus, v is the velocity of the dark matter particle and E_r is the recoil energy of the nucleus. Note that this is a spin-independent interaction, and hence is enhanced by Z, the total charge of the nucleus. The form factor $F(E_r)$ appearing here is the charge form factor of the nucleus. It has been

measured explicitly to be in good agreement with the Helm form factor [85]. The coefficient b_p is defined as

$$b_p = \frac{\lambda^2 e^2}{64\pi^2 m_\phi^2}\left[1 + \frac{2}{3}\log\left(\frac{m_\ell^2}{m_\phi^2}\right)\right]. \tag{4.2}$$

Here m_ℓ is the mass of the lepton in the loop, which has the same flavor as the dark matter particle. The leading logarithmic part of this expression was calculated in [84]. In the case of electron flavored dark matter, the mass of the lepton m_ℓ in Eq. 4.2 must be replaced by the momentum transfer $|\vec{k}|$ in the process, which we take to be 10 MeV as a reference value.

The magnetic dipole moment of the dark matter can also couple to the electric charge of the nucleus. This interaction is also spin-independent,

$$\frac{d\sigma_{DZ}}{dE_r} = \frac{e^2 Z^2 \mu_\chi^2}{4\pi E_r}\left[1 - \frac{E_r}{v^2}\frac{m_\chi + 2m_{nuc}}{2m_{nuc}m_\chi}\right] F^2(E_r)\ . \tag{4.3}$$

Finally, the dark matter can couple to the nuclear magnetic dipole moment via a dipole-dipole coupling. This interaction is spin-dependent, and therefore does not get an enhancement for large nuclei. It takes the form

$$\frac{d\sigma_{DD}}{dE_r} = \frac{m_{nuc}\,\mu_{nuc}^2\,\mu_\chi^2}{\pi v^2}\left(\frac{S_{nuc}+1}{3S_{nuc}}\right) F_D^2(E_r)\ , \tag{4.4}$$

where S_{nuc} is the spin of the nucleus, μ_{nuc} is its magnetic dipole moment, and $F_D(E_r)$ is the dipole moment form factor for the nucleus. There are currently no explicit measurements of the magnetic dipole form factor. A discussion of various form factors and an approximate calculation can be found in [86] (and references therein). The magnetic dipole moment of the dark matter particle μ_χ is related to

the model parameters by

$$\mu_\chi = \frac{\lambda^2 e\, m_\chi}{64\pi^2 m_\phi^2}\ . \tag{4.5}$$

Note that there is also a potential charge-dipole contribution to the cross section, where the dark matter vector bilinear couples to the magnetic dipole moment of the nucleus, but this interaction is suppressed by additional powers of momentum transfer.

The dipole-charge interaction is sub-dominant to the charge-charge interaction. The dipole-dipole coupling, being spin-dependent, is also sub-dominant. Consequently, we use the charge-charge cross section for placing limits. Then the scattering cross section can be approximated by,

$$\sigma^0_{ZZ} = \frac{\mu^2 Z^2}{\pi}\left[\frac{\lambda^2 e^2}{64\pi^2 m_\phi^2}\left[1+\frac{2}{3}\log\left(\frac{m_\ell^2}{m_\phi^2}\right)\right]\right]^2\ . \tag{4.6}$$

Here the superscript on σ^0_{ZZ} denotes that the cross section is at zero-momentum transfer, and μ is the reduced mass of the dark matter-nucleus system.

The ratio λ/m_ϕ corresponding to a thermal WIMP is plotted in Fig. 4.2 as a function of the dark matter mass, for the tau flavored and electron flavored cases. The current limits from the Xenon100 experiment [87] are also shown. It is clear from the figure that the expected improvement in sensitivity of the experiment by an order of magnitude will bring a large part of the parameter space of these models within reach.

In scenarios motivated by MFV, the splitting between the different states in the dark matter multiplet may be small enough that more than one state is present in the bath at freeze out. The observed dark matter may also be composed of more

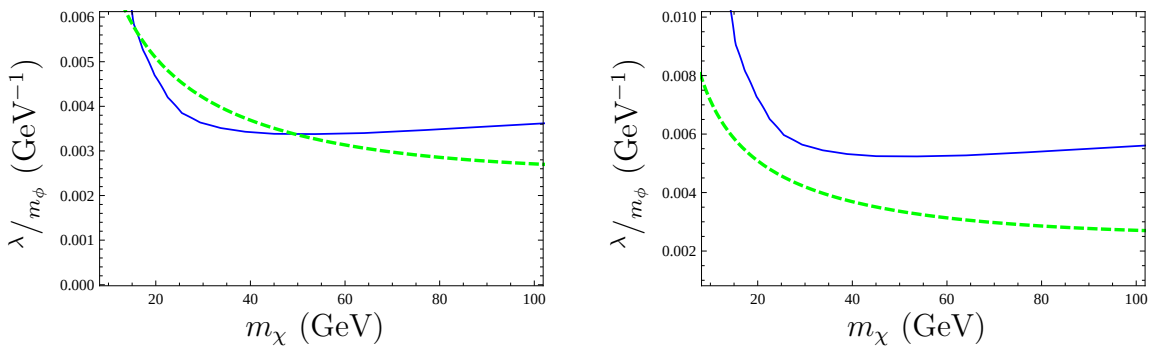

(a) (b)

Figure 4.2: Direct detection and relic abundance constraints on lepton flavor dark matter for a)χ_e and b)χ_τ, when $m_\phi = 150$ GeV. The area above the solid blue curve is ruled out by the new Xenon100 [87] data. The green dashed curves signify the parameters for which we obtain correct relic abundance.

than one flavor, if the splittings are small enough that the lifetimes of the heavier flavors are longer than the age of the universe. If all the dark matter flavors couple to the corresponding SM particles with the same strength, as when χ transforms under $\mathrm{U}(3)_E$, the calculation of the previous section shows that the parameters that give rise to the observed relic abundance are fairly insensitive to the number of dark matter species at freeze out. Therefore, if only one flavor constitutes all of dark matter today, the direct detection bounds are unchanged. This will be the case provided the lightest flavor, whether χ_e or χ_τ, is split from the others by a few tens of MeV or more. If more than one flavor constitutes the observed dark matter today, the bound may be obtained by appropriately interpolating between the somewhat different limits in the single flavor cases.

If, however, the quasi-degenerate dark matter flavors couple hierarchically, as

when χ transforms under $\mathrm{U}(3)_L$, the relic abundance calculation of the previous section shows that λ for the tau flavor is larger by a factor of $\sqrt{3}$ than in the single flavor case. In this scenario, if the observed dark matter is composed of the tau flavor, the limits are stronger by this factor than in the single flavor case. On the other hand, if dark matter today is composed of the e or μ flavors, the limits are much weaker than in the corresponding single flavor cases because of the hierarchical couplings of χ. The lightest flavor, whether χ_e or χ_τ, will constitute all of dark matter if it is split from the other states by a few hundred MeV or more. If more than one flavor constitutes the observed dark matter, the bound depends on the fraction of χ_τ, and may be obtained by interpolation.

If χ does transform under $\mathrm{SU}(2)_W$, we expect that the leading contribution to the cross section for dark matter scattering off a nucleus will arise from tree-level exchange of the SM Z, provided χ carries non-zero hypercharge. If χ arises from a representation which does not transform under hypercharge, then it does not couple directly to the Z, and so this effect does not arise. In this scenario, loop diagrams involving W bosons generate a contribution to the cross section [88] that must be compared against the contribution from the lepton loop above in order to determine the leading effect.

4.2 Quark Flavored Dark Matter

The direct detection signals of this class of models depend on the flavor of quark that the dark matter particle couples to, and on whether or not χ transforms under

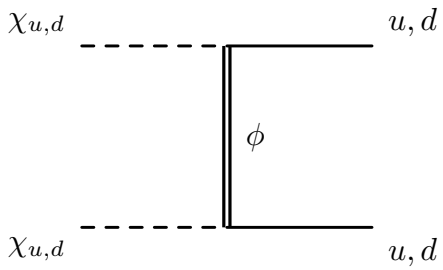

Figure 4.3: Diagram contributing to direct detection for dark matter coupling to first generation quarks.

the SM $SU(2)_W$ gauge symmetry. Consider first the case where χ is a SM singlet. In the region of parameter space relevant to current direct detection experiments, the matrix λ is constrained by flavor bounds to be closely aligned with the SM Yukawa couplings. We therefore concentrate on the case where λ is consistent with MFV. The relevant terms in the Lagrangian are then again those in Eq. 3.22.

MFV suggests that the lightest state in the dark matter multiplet carries either the flavor of a first generation quark, or a third generation quark. The direct detection signals are very different in the two cases, and so we consider them separately. For concreteness we begin by assuming that the different flavors of χ are not degenerate, and that a single dark matter flavor constitutes all the observed dark matter. We will relax this assumption later.

If dark matter carries up or down flavor, it can scatter off quarks in the nucleus at tree level by exchanging the mediator ϕ as shown in Fig. 4.3. Starting from the interaction in Eq. 3.22 we can integrate out the field ϕ, leading to the effective

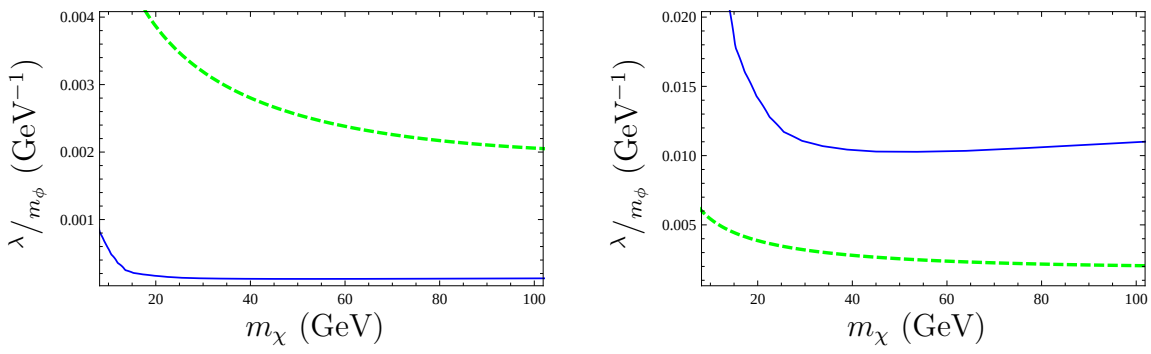

(a) (b)

Figure 4.4: Direct detection and relic abundance constraints on quark flavor dark matter for a) χ_u and b) χ_b, when $m_\phi = 150$ GeV. The area above the solid blue curve is ruled out by the new Xenon100 data [87]. The green dashed curves signify the parameters for which we obtain correct relic abundance.

operator

$$\frac{\lambda^2}{4m_\phi^2}\bar{\chi}(1+\gamma^5)q\ \bar{q}(1-\gamma^5)\chi\ . \tag{4.7}$$

After Fierz rearrangement, this operator becomes,

$$\frac{\lambda^2}{8m_\phi^2}\bar{\chi}\gamma^\mu(1-\gamma^5)\chi\ \bar{q}\gamma^\mu(1+\gamma^5)q\ . \tag{4.8}$$

The dominant contribution to direct detection comes from the spin-independent vector-vector coupling. The dark matter-nucleus cross section (at zero momentum transfer) in this case is given by [89]

$$\sigma^0 = \frac{\mu^2\lambda^4}{64\pi m_\phi^4}\left[A+Z\right]^2 \tag{4.9}$$

$$\sigma^0 = \frac{\mu^2\lambda^4}{64\pi m_\phi^4}\left[2A-Z\right]^2, \tag{4.10}$$

for dark matter coupling to up-type and down-type quarks respectively. Here μ represents the reduced mass of the dark matter-nucleus system, while Z and A are

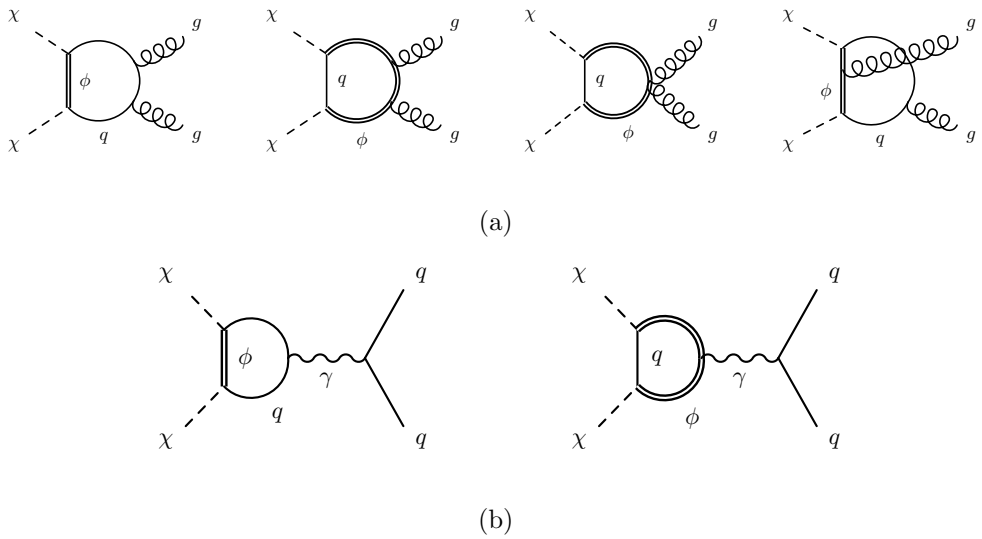

Figure 4.5: Diagrams contributing to direct detection for dark matter coupling to third generation quarks. The scattering can be off a) gluons and b) quarks via photon exchange. As discussed in the text, the photon exchange dominates for the example considered.

the atomic number and mass number of the nucleus. For a given value of λ, this cross section is much larger than in the leptonic case. In fact, as shown in Fig. 4.4(a), the region of parameter space where χ can be a thermal relic is already excluded by direct detection experiments.

We now move on to the case where the dark matter carries the flavor quantum numbers of third generation quarks. The contribution arising from Fig. 4.3 is now suppressed by mixing angles, and is expected to be sub-dominant. There is a possible contribution to the cross section arising from the one loop diagrams shown in Fig. 4.5(a), where χ scatters off gluons in the nucleus. However, it turns out that this is also not a significant effect. To understand why, we again integrate out the mediator ϕ at tree level to obtain the effective operator shown in Eq. 4.8. This

operator allows dark matter to scatter off a pair of gluons through triangle diagrams involving quarks. In general both the vector and axial vector terms in Eq. 4.8 contribute to the cross section. However, the contribution from the vector term vanishes identically as a consequence of the charge conjugation symmetries of QCD and QED (Furry's theorem) [90, 91]. The axial vector interaction couples dark matter to gluonic operators that are parity odd rather than parity even [90, 92]. The parity symmetry of QCD can be used to show that the matrix elements of these operators in the nucleus are either spin-dependent or velocity suppressed in the non-relativistic limit, and do not contribute significantly to dark matter scattering.

Thus, the dominant contribution to the cross section arises from one loop diagrams of the same form as in the lepton case, but now with the quarks running in the loop (Fig. 4.5 (b)). The cross sections will be identical except for factors of color and charge. As before, we only use the charge-charge interaction to calculate the bounds.

$$\sigma^0_{ZZ} = \frac{\mu^2 Z^2}{\pi}\left[\frac{3\lambda^2 e^2 Q}{64\pi^2 m_\phi^2}\left[1+\frac{2}{3}\log\left(\frac{m_q^2}{m_\phi^2}\right)\right]\right]^2, \tag{4.11}$$

where $Q = \frac{2}{3}, -\frac{1}{3}$ for top and bottom quarks respectively, and m_q is the mass of the quark in the loop. We see from Fig. 4.4(b) that the cross section corresponding to a thermal WIMP is within reach of current direct detection experiments.

Our MFV analysis shows that if the lightest state carries the up or down flavor, the mass splitting between the lightest two states in the dark matter multiplet is small enough that the next to lightest flavor plays a role in the relic abundance calculation. It may also be stable on cosmological time scales, and may contribute

to the observed dark matter density. It is therefore important to take this effect into account. Depending on the parameters, the dark matter flavors associated with the third generation may also play a role in determining the relic abundance. The analysis of the previous chapter shows that if dark matter transforms under $\mathrm{U}(3)_U$, the range of parameters that give rise to the correct relic abundance does not differ significantly from the single flavor case. It follows that if the lightest flavor is χ_u, this scenario is excluded, just as in the single flavor case. More generally, scenarios where χ_u constitutes a significant component of dark matter today are excluded. If χ_t is the lightest flavor, the other states will decay to it provided it is split from them by a few hundred MeV or more.

If dark matter transforms under $\mathrm{U}(3)_Q$, the couplings of χ are hierarchical, and so if the lightest state is associated with the first generation, it must be quasi-degenerate with the others to obtain the correct relic abundance. The analysis of the previous section then shows that if the splittings between these states are small compared to the freeze out temperature, the coupling λ corresponding to the third generation must be larger by a factor of $\sqrt{3}$ relative to the single flavor case. It follows that in this scenario, if the observed dark matter is composed of this flavor, the limits are stronger by the same factor than in the single flavor case. On the other hand, if dark matter today is composed of particles associated with the first generation, the limits are much weaker than in the corresponding single flavor case because of the hierarchical couplings of χ. In this realization of MFV, dark matter will be composed of only one flavor provided the lightest state is split from the others by more than a few GeV. If more than one flavor constitutes the

observed dark matter, the bound primarily depends on the constituent fraction of χ_t and may be obtained by interpolation. These considerations can be extended in a straightforward way to the other realizations of MFV.

If dark matter transforms non-trivially under the SM $\mathrm{SU}(2)_W$ symmetry, scattering processes via Z-boson exchange can give large direct detection signals. Consequently, these scenarios are expected to be severely constrained. However, if χ arises from a representation which does not transform under hypercharge, then it does not couple directly to the Z, and so this effect is absent. Then the effects of loop diagrams involving W bosons [88] must be compared against the contribution above in order to determine the leading effect.

Chapter 5

Collider Signals

The classes of flavored dark matter models considered in the thesis – quark and lepton flavored dark matter – predict a new particle ϕ charged under the SM gauge groups. Consequently, it could be produced at high energy colliders like the LHC, and potentially detected through its subsequent decays to SM particles. The characteristic signal of dark matter production is presence of missing energy (transverse momentum imbalance) in the final states.

In the following, we study the implications of FDM models for the LHC and probe features unique to these class of models. We then focus on a particular example, tau flavored dark matter, and consider in details its prospects for detection at the LHC.

5.1 Lepton Flavored Dark Matter

We focus on the scenario where dark matter couples flavor diagonally, and where the electron and muon flavored states in the dark matter multiplet are highly degenerate, as would be expected from MFV. In such a framework, the charged leptons that result from the decay of a muon flavored state to an electron flavored one (or vice versa) are extremely soft, and would be challenging to detect in an LHC environment. For the purposes of the following discussion, we will assume that these

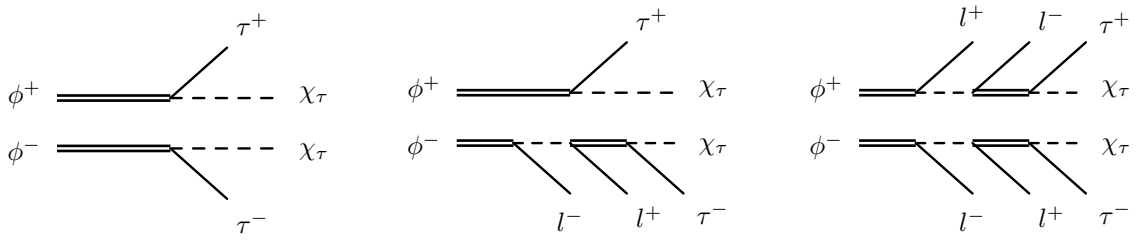

Figure 5.1: Signal topologies at colliders in models of tau flavored dark matter.

leptons are not detected. However, the splitting between a tau flavored state and an electron or muon flavored one is assumed to be large enough that the corresponding leptons can indeed be detected.

For concreteness, we limit ourselves to the case where χ does not transform under the SM $\mathrm{SU}(2)_W$ gauge interactions, and is a SM singlet. Then the mediator ϕ also does not transform under the $\mathrm{SU}(2)_W$ gauge symmetry. However, ϕ does have couplings to the photon and the Z boson, and can be pair-produced in colliders through an off-shell photon or Z. Each ϕ can then either decay directly to the dark matter particle, or decay to one of the heavier particles in the dark matter multiplet which then cascades down to the dark matter particle. Then, if the dark matter particle carries tau flavor, the decay of each ϕ results in either a single tau, or in two charged electrons/muons and a tau. Each event is therefore associated with exactly two taus, up to four additional charged leptons, and missing energy. These event topologies are shown in Fig. 5.1. If, on the other hand, the dark matter particle carries electron flavor, the decay of each ϕ will result in either a solitary electron or muon, or in two taus and an electron or muon. We therefore expect two electrons,

two muons or an electron and a muon in each event, along with missing energy and up to four taus.

5.2 Quark Flavored Dark Matter

The collider signals of this class of theories differ depending on whether the dark matter particle couples primarily to the third generation quarks, or to the quarks of the first two generations. We will restrict our discussion to the case where the couplings of χ are consistent with MFV. As before, the dark matter particles are assumed to be SM singlets, so ϕ does not carry $\mathrm{SU}(2)_W$ quantum numbers, however it does carry color quantum numbers. Our results can be extended to the more general case without difficulty. The mediators ϕ can be pair-produced at the LHC through QCD, and each will decay down to the dark matter particle either directly, or through a cascade. If the dark matter particle belongs to the third generation, at the partonic level each event is associated with two heavy flavor quarks and up to four light quarks. If, on the other hand, it belongs to the first generation, we expect between zero and four heavy flavor quarks in each event, along with two light quarks.

5.3 Collider Signals of Tau Flavored Dark Matter

In this section we discuss in detail the collider signals of a specific model in which the dark matter particle carries quantum numbers under tau flavor. For concreteness we assume that the dark matter particle is a Dirac fermion which is a singlet under weak

interactions, and therefore does not transform under the $\mathrm{SU}(2)_W$ gauge interactions of the SM.

Dark matter couples directly to the SM through interactions of the form

$$\mathcal{L} = \sum_{i=e,\mu,\tau} \left[\lambda^i_j \, E^c{}_i \chi^j \, \phi \; + \mathrm{h.c.} \right], \tag{5.1}$$

where ϕ is the mediator, and $\chi_{e,\mu,\tau}$ are the dark matter and its copies. This interaction fixes the SM quantum numbers of ϕ, which is charged under the photon and the Z, but does not couple to the W.

We consider two benchmark spectra that are consistent with MFV, with χ transforming under $\mathrm{U}(3)_E$. Then χ_e and χ_μ are expected to be nearly degenerate since the corresponding SM Yukawa couplings are very small. We assume that χ_τ is lighter than χ_e or χ_μ, and constitutes dark matter.

We label the first benchmark spectrum τFDM1:

$$\begin{aligned} m_{\chi,e} &= 110 \text{ GeV} \\ m_{\chi,\mu} &= 110 \text{ GeV} \\ m_{\chi,\tau} &= 90 \text{ GeV} \\ m_{\phi} &= 160 \text{ GeV}. \end{aligned} \tag{5.2}$$

The second benchmark spectrum we study has a lighter mediator, and therefore leads to a larger production cross section (see Fig 5.2). We label this benchmark

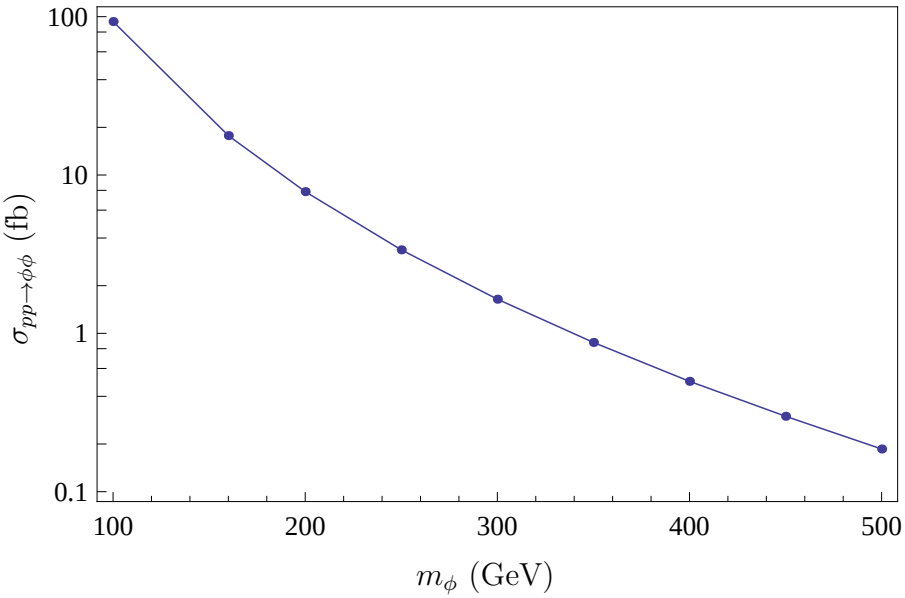

Figure 5.2: Pair-production cross section for the mediator ϕ in τFDM at the 14 TeV LHC run as a function of its mass.

spectrum τFDM2:

$$m_{\chi,e} = 90 \text{ GeV} \tag{5.3}$$

$$m_{\chi,\mu} = 90 \text{ GeV}$$

$$m_{\chi,\tau} = 70 \text{ GeV}$$

$$m_\phi = 150 \text{ GeV}.$$

In these simple models, only the mediator ϕ carries SM gauge quantum numbers, so dark matter events at colliders must arise from $\phi^+\phi^-$ production. The ϕ particles then decay, either directly or via cascade decays, into SM charged leptons and the dark matter particle. Thus, the characteristic signature of this model is leptons+MET.

As discussed earlier, MFV restricts the matrix λ to be approximately pro-

portional to identity. Consequently, we take the couplings of different dark matter flavors to SM to be equal, their common value set by the relic abundance requirement. Collider signals are insensitive to this value.

Since $\phi^+\phi^-$ production proceeds through Drell-Yan and ϕ is a scalar, the ϕ pair comes out in a p-wave, leading to a small cross section, on the order of 10 fb at the 14 TeV LHC run. Therefore, we do not expect the early LHC data to be able to probe this model. In order to obtain reasonable signal over background discrimination, tens of inverse fb of data will be required.

5.3.1 Signal Topologies

Signal events come in three distinct topologies (see Fig. 5.1). Each ϕ can decay directly into the dark matter particle and a τ, corresponding to a short chain. Alternatively, it can decay to one of the heavier particles in the dark matter multiplet, which eventually cascades down to the dark matter particle, creating a long chain. Therefore each event can be categorized as comprising of short-short, short-long or long-long chains.

Since τ's are difficult to identify, we implicitly restrict ourselves to $\ell = e, \mu$ final states in this section when we talk about leptons. The events with the long-long decay chain topology have four-lepton final states (not to mention a pair of τ's), which have small SM backgrounds. When χ is Majorana rather than Dirac, the short-long chain will also include a like-sign dilepton final state which is a very clean signal. The τ's in the event could also decay leptonically, giving rise to additional

leptons. However, these leptons are generally softer than the primary leptons. In principle, with additional leptons in the event, identification of τ's is also possible. However, in this thesis we focus on the long-long decay topology, and do not take advantage of τ identification.

In order to simulate signal and background events we use the usrmod utility of MadGraph/MadEvent [93, 94], and we use BRIDGE [95] for the $\chi_{e,\mu}$ decays. Pythia [96] is used to simulate parton showers and hadronic physics, and PGS [97] with the default CMS parameter set is used to simulate detector effects.

5.3.2 Backgrounds

While four-lepton final states are rare in the SM, the signal cross section is also small so we carefully consider the three leading sources of backgrounds and devise cuts to reduce them as much as possible.

$(Z/\gamma)^{(*)}(Z/\gamma)^{(*)}$

One of the dominant backgrounds is production of two opposite-sign, same-flavor lepton pairs from either on-shell or off-shell Z's and photons. Missing energy in this background arises from mis-measurement of lepton momenta, which is small. In general, there is also contribution to missing energy from the underlying event, which we do not consider in the present analysis. For the following contributions to this background, we choose the following cuts:

- $Z \to \ell^+\ell^-$: This is the dominant component in this background, which we

reduce by imposing a Z-veto (described in the next subsection)

- $Z \to \tau^+\tau^- \to \ell^+\ell^-$: Even though the Z is on-shell in this process, the Z-veto is not effective due to the presence of neutrinos in the final state. This contribution is small due to the leptonic τ branching ratios. The leptons arising from τ decays are also softer, which we reduce by demanding the leptons to be energetic.

- $Z^*/\gamma^* \to \ell^+\ell^-$: While the off-shell production cross section is much smaller than on-shell production, this is the main contribution that remains after the Z-veto and lepton energy cuts. We impose a missing energy cut to reduce this background component.

$t\bar{t}(Z/\gamma)^{(*)}$

This background process, while it has a three-body final state, has a cross section comparable to the above process which is purely electroweak. When both tops decay leptonically and the $(Z/\gamma)^{(*)}$ goes to leptons, the final state is 4ℓ+jets+MET. The Z-veto reduces the on-shell Z production, and we also impose a dijet veto (described in the next subsection) in order to reduce this background, since signal events will typically not have any hard jets.

$WW(Z/\gamma)^{(*)}$

This process is qualitatively similar to the above process, but has a much smaller production cross section because it is purely electroweak. On the other hand, there

are no additional hard jets in these events, so they escape the dijet veto. Consequently, events which escape the Z-veto can fake the four-lepton signal very well. Demanding the leptons to be energetic and imposing the missing energy cut helps reduce this background.

Backgrounds with fakes

There are also backgrounds arising from jets that are misidentified as leptons. We find that provided the fake rates are of order 10^{-3} or less, the irreducible backgrounds described above are the dominant ones.

5.3.3 Cuts

We use the following cut flow in order to maximize signal over background:

- Lepton cuts - We demand events with at least four leptons with $pT > 7$ GeV each. At least two of these leptons are further required to have $E > 50$ GeV.
- Dijet veto - We discard events with two or more jets of $pT > 30$ GeV each.
- Z veto - We veto events if the invariant mass of any Z-candidate (a pair of same-flavor and opposite-charge leptons) falls within 7 GeV of the Z mass. This is a tighter Z-veto than is usually used, but we find that the loss in signal efficiency is more than compensated for by the background reduction.
- Missing energy - We require at least 20 GeV of missing energy in each signal event. Since most backgrounds with high MET have already been eliminated

Dataset	Event rate after cuts at 100 fb^{-1}			
	Lepton cuts	Jet cuts	Z veto	MET
τFDM1	46.73	42.83	38.41	35.01
τFDM2	75.39	69.30	63.26	57.04
$\ell^+\ell^-\ell^+\ell^-$	1617.94	1582.42	140.30	13.32
$t\bar{t}\,\ell^+\ell^-$	89.57	19.45	4.92	4.70
$WW\ell^+\ell^-$	14.70	13.98	2.51	2.51

Table 5.1: Signal and SM background event rates for processes yielding 4-lepton final states after each set of cuts is progressively applied (note that $\ell = e, \mu$). All numbers are reported for the 14 TeV LHC run and include detector effects.

by the previous cuts in the cut flow, we find that a mild threshold such as 20 GeV is sufficient. We have not considered backgrounds due to pile-up, which might require a higher missing energy cut.

5.3.4 Results

The signal and background events of each type that survive these cuts are listed in Table 5.1. These results show that it is possible to discover the τFDM2 benchmark above SM backgrounds at 5σ significance with about 20 fb^{-1} of data at the 14 TeV LHC run. A higher luminosity (~ 40 fb^{-1}) would be needed in order to distinguish the τFDM1 benchmark from the SM background. Note that while we have based this expectation on statistical uncertainties only, we have been conservative in many other aspects. In particular, a requirement that each event have at least one τ candidate would virtually eliminate all remaining backgrounds while reducing the signal only moderately. Furthermore, one could do better than a pure counting

experiment by taking into account the charge and flavor correlations present in the signal, which are different than the backgrounds in order to further increase sensitivity. We will indeed use this approach in the next section where we consider how the FDM model could be distinguished from more conventional DM models where the dark matter particle is a flavor singlet.

While ATLAS [98] and CMS [99] have already performed searches in multi-lepton final states, considering the low cross section of the FDM benchmark model, they are not yet expected to have exclusion level sensitivity to this scenario.

5.4 Distinguishing τFDM

Multi-lepton events with large missing energy are fairly common signals in theories with neutral stable particles and partners to the SM leptons, which include a variety of dark matter models. We would to like understand whether it is possible to distinguish at the LHC the model of τFDM that we studied in the previous section from models with similar signatures but where the dark matter does not carry flavor quantum numbers. Clearly, this question is very difficult in general. Therefore, we focus on a more restricted question. We investigate whether it is possible to distinguish τFDM from a specific 'strawman' model, where the dark matter does not carry flavor.

The strawman model we choose is related to supersymmetric theories where the bino constitutes dark matter. The form of the lepton-slepton-bino vertex is very similar to the defining vertex of a theory of lepton FDM (LFDM), except that in the

supersymmetric case it is the slepton that carries flavor, not the bino. We choose the strawman model to consist of the bino, which we label by χ, along with the three right-handed sleptons, $\widetilde{E}_i^c$. The bino constitutes dark matter. To mimic the collider signals of τFDM, we add to the strawman model an additional 'neutralino' χ', which is heavier than the bino. χ' is an admixture of a SM $\mathrm{SU}(2)_W$ doublet and singlet, so that it can be pair-produced through the Z, and is chosen to couple to leptons and sleptons in a flavor-blind way. This interaction takes the schematic form

$$\lambda' E_i^c \chi' \widetilde{E}^{c\,i} \quad + \quad \text{h.c.} \tag{5.4}$$

The couplings of χ' are somewhat different from those of a conventional neutralino in the MSSM, since any neutralino with significant couplings to the Z is expected to contain a significant Higgsino component, and the Higgsino does not couple universally to the different leptons. However, this simple strawman model captures the main features of theories where the dark matter does not carry flavor, while generating events which are very similar to those of τFDM.

For simplicity, in what follows we assume that the three sleptons are degenerate in mass. In general, χ' could either be lighter than or heavier than the sleptons, while the bino is the lightest of the new states. Both χ' and χ are taken to be Majorana fermions as is the case in the MSSM.

Signal events in the τFDM model involve four or more isolated leptons and missing energy. The strawman model can generate similar events through sleptons pair-production in colliders. If they are heavier than χ', this leads to events of the

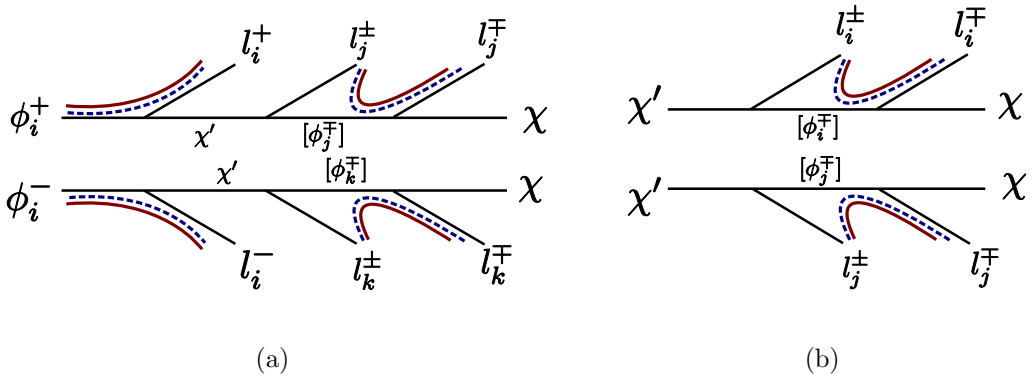

(a) (b)

Figure 5.3: Flavor (red solid) and charge (blue dashed) correlations are shown for topologies in strawman models.

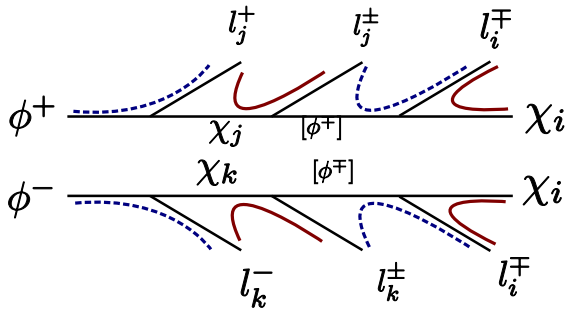

Figure 5.4: Flavor (red solid) and charge (blue dashed) correlations are shown for τFDM. Final state lepton charge ambiguities for Majorana dark matter models do not affect the charge correlation.

form shown in Fig. 5.3(a), which involve six leptons, any or all of which could be taus. We label this possibility topology (a). Two χ' particles can also be pair-produced, leading to events of the form shown in Fig. 5.3(b), which we label topology (b). These events involve four leptons, any or all of which could be taus.

How can we distinguish between signal events in the two classes of models? One possibility is to note that we expect exactly two taus in each signal event in the τFDM model, whereas events in the strawman models will involve between zero and six. This could be a useful discriminant as the LHC experiments continue to improve their τ identification capabilities. Presently, we do not make use of this discriminant. We also do not assume that the total event rate will be a reliable variable for discrimination. Even though in principle the event rate can vary widely across different models, for the following analysis we simply scale the event rate from the strawman model to match the number of events from τFDM and concentrate on ratios and asymmetries.

In particular, we focus on charge and flavor correlations among the final state leptons in the event. In Fig. 5.3 and Fig. 5.4, we exhibit the correlation of flavor and charge among the final state leptons in signal events for the τFDM model and the strawman model. The crucial observation is that, in the case of τFDM, for the chosen spectrum, the two upstream leptons are also the hardest. This is likely to be the case for spectra motivated by MFV. These leptons are charge anti-correlated since they arise from the decay of the charged mediators ϕ. However, they have no flavor correlation, because the mediator does not carry flavor quantum numbers.

Contrast this with the strawman model. Consider first events associated with

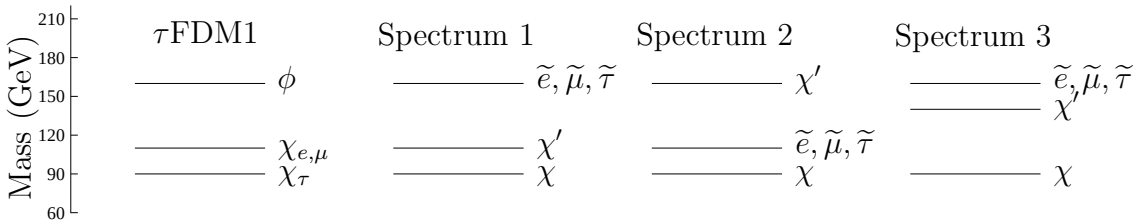

Figure 5.5: The FDM spectrum and the strawman spectra compared.

topology (a). If the mass of ϕ is much larger than that of χ', the two upstream leptons in the event are the hardest. These exhibit charge anti-correlation, but are flavor correlated, in contrast to τFDM. If, on the other hand, the mass of ϕ is close to that of χ', two of the four downstream leptons will be the hardest. However, these exhibit no significant charge or flavor correlation, unlike τFDM. The events associated with topology (b) have the two hardest leptons charge and flavor uncorrelated. We conclude from this that the charge and flavor correlations are different in the two theories, and may allow them to be distinguished.

We generated signal events for the strawman model for three benchmark spectra, shown schematically in Fig. 5.5, and compared the resulting charge and flavor correlations to those of τFDM. In particular, the spectra we studied were the following.

Spectrum 1

We assume the masses of the sleptons to be the same as that of the mediator ϕ in τFDM. The masses of χ' and χ are also chosen equal to the $\chi_{e,\mu}$ and χ_τ mass

respectively,

$$m_{\chi'} = 110 \text{ GeV} \tag{5.5}$$

$$m_{\chi} = 90 \text{ GeV}$$

$$m_{\widetilde{e},\widetilde{\mu},\widetilde{\tau}} = 160 \text{ GeV}.$$

This spectrum can clearly give rise to both topologies in Fig. 5.3, but since the mass splitting between χ and χ' is small, events from topology (b) generally fail to pass the four-lepton cut requiring two leptons to have more than 50 GeV energy. Therefore, topology (a) dominates the phenomenology of this benchmark.

In this topology, the two most upstream leptons are also the hardest, *and* are flavor-correlated. The τFDM leptons, as noted above, have no flavor correlation. Therefore, we expect that the flavor-correlation of the two hardest leptons is a good discriminant in this case.

Spectrum 2

If the mass of the sleptons is less than the mass of χ', then only the topology (b) is allowed. The decay of χ' is on-shell in this case.

The representative spectrum we study is,

$$m_{\chi'} = 160 \text{ GeV} \tag{5.6}$$

$$m_{\chi} = 90 \text{ GeV}$$

$$m_{\widetilde{e},\widetilde{\mu},\widetilde{\tau}} = 110 \text{ GeV}.$$

In this case, the hardest leptons should exhibit neither charge nor flavor correlations, allowing us to distinguish it from τFDM.

Spectrum 3

Consider again the case when the mass of χ' is less than mass of χ. As noted in the case of Spectrum 1, when the mass of χ' is close to the mass of χ, topology (a) dominates. On the other hand, when the mass of the χ' is very close to the mass of sleptons, the most upstream leptons become softer, and topology (b) dominates. The conclusions in this case are then identical to those of Spectrum 2.

In the intermediate case, however, the result is a mixture of the two topologies. In order to investigate this we study a third spectrum,

$$m_{\chi'} = 140 \text{ GeV} \tag{5.7}$$

$$m_{\chi} = 90 \text{ GeV}$$

$$m_{\widetilde{e},\widetilde{\mu},\widetilde{\tau}} = 160 \text{ GeV}.$$

In the next section we study the extent to which each of these spectra can be distinguished from τFDM.

5.4.1 Comparison

The correlations we obtain are listed in Table 5.2. The results are in agreement with our expectations. Events with topology (a) in Spectrum 1 clearly exhibit flavor correlation between the two hardest leptons, as expected for the upstream leptons created from (flavor-carrying) sleptons. On the other hand, τFDM exhibits no flavor correlation in the hardest two leptons.

In all the fake spectra with topology (b), the two hardest leptons show no preferential charge assignment beyond the ratio of 1 : 2 for same to opposite charge, as

Dataset	Frac. events with same	
	Flavor	Charge
τFDM1	0.52	0.14
τFDM2	0.49	0.14
Spectrum 1(a)	0.87	0.13
Spectrum 1(b)	0.61	0.39
Spectrum 2	0.55	0.41
Spectrum 3(a)	0.66	0.33
Spectrum 3(b)	0.60	0.38

Table 5.2: Flavor and charge correlations for the two highest p_{T} leptons in events passing cuts for different data samples. The strawman models are represented by the spectrum and their event topology.

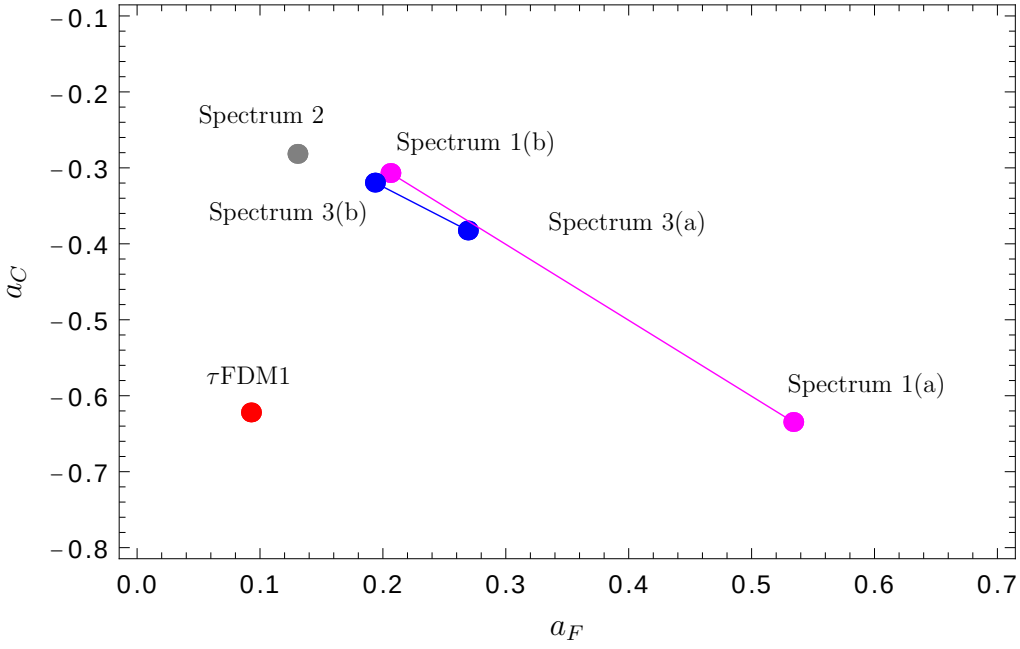

Figure 5.6: Flavor and charge asymmetry for different models and event topologies. The straight lines interpolate between points which correspond to different event topologies for each fake spectrum, in order to account for cases where both topologies contribute.

expected from random charge assignment. Consequently these cases have a weaker charge anti-correlation than the τFDM.

Events from topology (a) in Spectrum 3 fall in the middle, with somewhat significant charge anti-correlation, and a weak flavor correlation. While the correlation between charge and flavor is different from the τFDM case, higher statistics might be needed in this case to make a precise distinction. We also illustrate these results in Fig. 5.6. We plot the flavor and charge asymmetries of the two hardest leptons for FDM and the strawman spectra, taking into account the contributions from SM backgrounds. The charge and flavor asymmetries are defined as

$$a_F, a_C = \frac{n_{\text{same}} - n_{\text{diff.}}}{n_{\text{same}} + n_{\text{diff.}}} \ . \tag{5.8}$$

A large amount of data is required to distinguish between the FDM and the strawman spectra at a high statistical significance. A log-likelihood analysis shows that a luminosity of 200 fb^{-1} at the 14 TeV LHC allows one to distinguish the FDM model from each one of the strawman spectra by at least 95% confidence-level [8].

Note that while we have relied only on the energies of the leptons to help us identify the topology of the event, this is just the simplest approach and can be extended with more sophisticated tools. For example, when applicable, the hemisphere algorithm [100] can distinguish particles arising from different decay chains, and has been used widely for this purpose [101, 102, 103]. There have also been other techniques proposed to help identify event topologies [104, 105]. Additionally, one can make use of further ratios involving the softer leptons to obtain better discrimination between these models.

Chapter 6

Conclusions

Observations of the universe indicate the presence of dark matter. However, a microscopic theory of dark matter is still missing. A dark matter which is a thermal relic neatly fits into the WIMP paradigm, with a weak scale mass and weak scale interactions with ordinary matter. The hierarchy problem in the SM suggests new physics at the weak scale. Therefore, it is possible that the dark matter particles are part of this new physics sector, and can be discovered at present day experiments.

Experimental signatures can depend sensitively on dark matter properties, and thus it is important to study many distinct realizations of dark matter. Traditionally, dark matter has been studied as a by-product of a larger new physics sector. Consequently, searches for dark matter have been restricted to parameter spaces predicted within these new physics frameworks.

In this thesis, we have studied a novel possibility that dark matter particles carry flavor quantum numbers. Some particular realizations of this structure have been explored in the literature, e.g. sneutrino dark matter in Supersymmetric (SUSY) theories and KK-neutrino dark matter in theories with an extra dimension. However, there is a large theory space left unexplored in this paradigm.

To study these models, the flavor symmetry of the SM is extended to include a new flavor symmetry under which the dark matter transforms. The models are

classified based on whether the dark matter flavor is identified with quark or lepton flavor, or if it is independent of SM matter flavor. Each of these possibilities is associated with a characteristic type of vertex, leading to different predictions for direct detection experiments and to distinct collider signatures. In particular, assuming a coupling consistent with relic abundance considerations, we have shown that many of these models could be probed in the near future by upcoming direct detection experiments.

We have further studied in detail a class of models where dark matter carries tau flavor, where the collider signals include events with four or more isolated leptons and missing energy. We have performed a full simulation of the signal and SM backgrounds, including detector effects, and shown that in a significant part of the parameter space favored by MFV, these theories can be discovered above SM backgrounds at the 14 TeV LHC run. We have also shown that flavor and charge correlations among the final state leptons may allow models of this type to be distinguished from simple theories where the dark matter particle couples to leptons but does not carry flavor.

Our analysis is a first step in uncovering a vast array of possibilities. There are many different directions in which this research can be extended. We list a few below,

- We have focused on a subset of models in this thesis, particularly those under which the dark matter is an electroweak singlet. The case where dark matter particle has electroweak charge deserves further study.

- We have explored the phenomenology of FDM models at direct detection and collider experiments, and assumed a structure which makes them safe from flavor constraints. It will be interesting to generalize the analysis and to carry out a detailed study and predictions for flavor experiments associated with different FDM models.

- The flavor structures associated with the dark matter particles and the mediators were chosen based on minimality, and many more general possibilities exist.

- Our collider study was designed to be conservative in order to robustly show the discovery potential of such models. To extract the most significance from collider data, more sophisticated tools can be employed for the detection of the model and distinguishing it from other models where the dark matter particles do not carry flavor.

- For concreteness, we restricted detailed collider analysis to one particular example of FDM. It would be valuable to consider other models outlined in this thesis in a detailed collider analysis.

We have indirect evidence for physics beyond the Standard Model in the form of dark matter. There are a number of active experiments probing theoretically well-motivated parameter space of many dark matter models. There is great hope that current and future experiments will uncover the mysterious properties of dark matter over the next decade.

Appendix A

Direct Detection of Lepton Flavored Dark Matter

In this appendix we calculate the contribution to the cross section for dark matter scattering off a nucleus arising from the diagram shown in Fig. 4.1.

Our approach will be to integrate out the mediator ϕ and the leptons l in the loop to obtain an effective vertex for the coupling of the dark matter particle χ to the photon. The resulting effective theory, which can be used to directly obtain the cross section, is valid provided the momentum transfer $|\vec{k}|$ in the process is smaller than the mass of the lepton in the loop. The momentum transfer in direct detection experiments is typically of order 10 - 50 MeV, which implies that this procedure is valid if the lepton in the loop is the muon or the tau, but not if it is the electron. However, the final result can generalized to obtain an expression that is approximately valid for this case as well.

We first identify the operators that can potentially appear in the effective vertex. We begin by noting that the vertices in the diagrams in Fig. A.1 do not by themselves violate CP symmetry. We therefore write down the leading effective operators that couple dark matter to the photon, and which are consistent with electromagnetic gauge invariance and CP. The lowest dimension operator consistent with these symmetries is unique. It is the dimension-5 dipole moment operator,

$$\bar{\chi}\sigma_{\mu\nu}\chi \; F^{\mu\nu} \; . \tag{A.1}$$

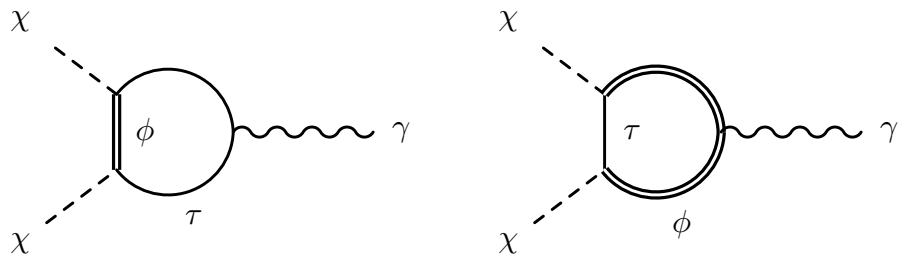

Figure A.1: Dark matter interaction with a photon in the full theory.

However, this operator does not actually appear in the effective theory. The underlying reason is that this operator breaks the chiral symmetry of the χ field. All the vertices and propagators in Fig. A.1 respect this symmetry, while the mass term of χ, which breaks it, does not appear in the diagrams. This is most easily seen if we first integrate out just the heavy mediator ϕ and consider the resultant effective four-fermion operator,

$$\bar{\chi}(1+\gamma_5)\ell\ \bar{\ell}(1-\gamma_5)\chi\ . \tag{A.2}$$

A Fierz rearrangement shows that this is equivalent to the operator

$$\bar{\chi}\gamma^\mu(1-\gamma_5)\chi\ \bar{\ell}\gamma_\mu(1+\gamma_5)\ell\ , \tag{A.3}$$

which establishes that the dark matter coupling is indeed chiral. Hence, we do not generate the dipole interaction above after integrating out the lepton.

As a consequence, the leading contribution to the dark matter-nucleus scattering arises from dimension-6 operators. Again, gauge and CP symmetries, together with the chiral symmetry mentioned above, restrict us to the following two opera-

tors,

$$\mathcal{O}_1 = \left[\bar{\chi}\gamma^\mu(1-\gamma^5)\partial^\nu\chi \ + h.c.\right] F_{\mu\nu} \tag{A.4}$$

$$\mathcal{O}_2 = \left[i\bar{\chi}\gamma^\mu(1-\gamma^5)\partial^\nu\chi \ + h.c.\right] F^{\sigma\rho}\epsilon_{\mu\nu\sigma\rho} \ . \tag{A.5}$$

The factors of i in the definitions of these operators have been chosen so that their coefficients in the effective theory are necessarily real.

To calculate the coefficients of these operators in the effective theory we perform a matching calculation from the full theory to the effective theory, where the mediator ϕ and the lepton l have been integrated out.

In 4-component Dirac notation the relevant part of the Lagrangian in the full theory takes the form

$$\mathcal{L} \supset \frac{\lambda}{2}\left[\bar{\chi}(1+\gamma_5)\ell\ \phi + \bar{\ell}(1-\gamma_5)\chi\ \phi^\dagger\right] \ . \tag{A.6}$$

We can compute the one loop processes shown in Fig. A.1 to find the low energy effective Lagrangian. Since we are interested in direct detection processes with momentum transfer of at most $\mathcal{O}(100\text{ MeV})$, we only work to $\mathcal{O}(k^2/m_\phi^2)$ in momentum transfer. Further, we only keep the leading term in m_ℓ/m_ϕ, which is a good approximation in our case. In this limit, the amplitude in the full theory is given by,

$$\begin{aligned}\mathcal{M} = \frac{\lambda^2 e}{64\pi^2 m_\phi^2}&\bar{u}(p_2)\gamma_\delta(1-\gamma^5)u(p_1)\epsilon_\mu^*(k) \\ &\times\left[k^2\left(\frac{1}{2}+\frac{2}{3}\log\left[\tfrac{m_\ell^2}{m_\phi^2}\right]\right)g^{\mu\delta} - \frac{i}{2}(p_1+p_2)_\alpha k_\beta\epsilon^{\alpha\mu\beta\delta}\right],\end{aligned} \tag{A.7}$$

where p_1, p_2 and k are the momenta of the incoming dark matter, outgoing dark matter, and the photon, respectively. Using integration by parts on the operators

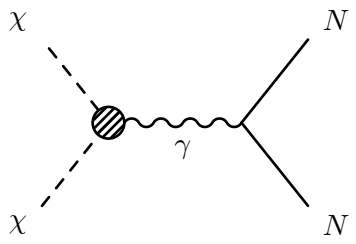

Figure A.2: Direct detection diagram for the dark matter in the effective theory.

shown above, we see that the term with k^2 corresponds to $\mathcal{O}_1$, and the second term corresponds to $\mathcal{O}_2$. Matching the coefficients, we can write down the effective Lagrangian,

$$\mathcal{L}_{eff} = \frac{-\lambda^2 e}{64\pi^2 m_\phi^2}\left[\left(\frac{1}{2}+\frac{2}{3}\log\left[\tfrac{m_\ell^2}{m_\phi^2}\right]\right)\mathcal{O}_1+\frac{1}{4}\mathcal{O}_2\right]. \tag{A.8}$$

We can now calculate the amplitudes for scattering of dark matter with nuclei arising from these different effective operators and investigate their qualitative behavior. The scattering amplitude due to the first operator is given by,

$$\mathcal{M}_{\mathcal{O}_1} = \sum_q \frac{\lambda^2 e^2}{64\pi^2 m_\phi^2}\left(\frac{1}{2}+\frac{2}{3}\log\left[\tfrac{m_\ell^2}{m_\phi^2}\right]\right)\bar{u}(p_2)\gamma^\mu(1-\gamma^5)u(p_1)\,\langle N|Q\,\bar{q}\gamma_\mu q|N\rangle\ , \tag{A.9}$$

where we sum the matrix elements of all quark bilinears in the nucleus, and Q is the charge of the quark in units of e. This is the typical interaction through the vector current. This gives rise to predominantly spin-independent cross sections which are enhanced for large nuclei.

Consider the scattering amplitude due to the second operator,

$$\mathcal{M}_{\mathcal{O}_2} = -\sum_q \frac{i\lambda^2 e^2}{32\pi^2 m_\phi^2}\bar{u}(p_2)\gamma^\mu(1-\gamma^5)u(p_1)\,\frac{(p_2+p_1)^\nu k^\alpha}{4k^2}\langle N|Q\,\bar{q}\gamma^\beta q|N\rangle\epsilon_{\mu\nu\alpha\beta}\ . \tag{A.10}$$

To disentangle different contributions, we use the Gordon identity on the dark matter spinors. Since we are using the equation of motion of the dark matter particle, we will now generate chiral symmetry-violating bilinears as well ($\bar{u}\,\sigma^{\alpha\beta}u$ in particular). Neglecting terms of higher order in momentum transfer and relative velocity, we get,

$$\begin{aligned}\mathcal{M}_{\mathcal{O}_2} = &-\frac{i\lambda^2 e^2}{64\pi^2 m_\phi^2 m_\chi}\frac{(p_1+p_2)_\omega(p_2+p_1)^\nu k^\alpha}{4k^2}\\ &\times\bar{u}(p_2)\left[i\sigma^{\omega\mu}\gamma_5\right]u(p_1)\sum_q\langle N|Q\,\bar{q}\gamma^\beta q|N\rangle\epsilon_{\mu\nu\alpha\beta}\ .\end{aligned} \tag{A.11}$$

We can rewrite $\sigma^{\omega\mu}\gamma^5$ as $\frac{i}{2}\sigma_{\delta\rho}\epsilon^{\omega\mu\delta\rho}$ and contract the Levi-Civita tensors. Using Gordon's identity again, the resulting expression can be brought to the following form,

$$\mathcal{M}_{\mathcal{O}_2} = -\frac{i\lambda^2 e^2}{64\pi^2 m_\phi^2}\sum_q\langle N|Q\,\bar{q}\gamma_\alpha q|N\rangle\left[m_\chi\bar{u}(p_2)\sigma^{\alpha\beta}u(p_1)\frac{k_\beta}{k^2}+\frac{i}{2}\bar{u}(p_2)\gamma^\alpha u(p_1)\right]. \tag{A.12}$$

Combining both operators, the total scattering amplitude is

$$\mathcal{M} = \sum_q\left[\mu_\chi e\bar{u}(p_2)\sigma^{\alpha\beta}u(p_1)\frac{ik_\alpha}{k^2}\langle N|Q\,\bar{q}\gamma_\beta q|N\rangle + b_p\bar{u}(p_2)\gamma^\beta u(p_1)\langle N|Q\,\bar{q}\gamma_\beta q|N\rangle\right]\ , \tag{A.13}$$

where we have defined

$$\mu_\chi = \frac{\lambda^2 e m_\chi}{64\pi^2 m_\phi^2} \tag{A.14}$$

$$b_p = \frac{\lambda^2 e^2}{64\pi^2 m_\phi^2}(1+\frac{2}{3}\log\left[\tfrac{m_t^2}{m_\phi^2}\right])\ , \tag{A.15}$$

and neglected the velocity-suppressed contribution from $\mathcal{M}_{\mathcal{O}_1}$.

The first term in the amplitude corresponds to the magnetic dipole moment of χ interacting with the nucleus, and the second term is the familiar charge-charge interaction. The dipole couples to both the charge of the nucleus and its magnetic dipole moment. The momentum-transfer dependence of each of these terms is different. The dipole-charge interaction is enhanced at low-momentum transfers due to the presence of the k_α/k^2 factor. However, the coupling to the dipole moment of the nucleon involves an additional power of the momentum transfer k. Therefore the dipole-dipole interaction has no such enhancement and exhibits the same recoil spectrum as the charge-charge interaction up to form factors.

We show the three components of the scattering cross section: charge-charge (σ_{ZZ}), dipole-charge (σ_{DZ}) and dipole-dipole (σ_{DD}) [106, 86]. The differential scattering cross sections with respect to the recoil energy E_r, are given as follows,

$$\frac{d\sigma_{ZZ}}{dE_r} = \frac{2m_{nuc}}{4\pi v^2} Z^2\, b_p^2\, F^2(E_r) \tag{A.16}$$

$$\frac{d\sigma_{DZ}}{dE_r} = \frac{e^2 Z^2 \mu_\chi^2}{4\pi E_r}\left[1 - \frac{E_r}{v^2}\frac{m_\chi + 2m_{nuc}}{2m_{nuc}m_\chi}\right] F^2(E_r) \tag{A.17}$$

$$\frac{d\sigma_{DD}}{dE_r} = \frac{m_{nuc}\,\mu_{nuc}^2\,\mu_\chi^2}{\pi v^2}\left(\frac{S_{nuc}+1}{3S_{nuc}}\right) F_D^2(E_r)\ . \tag{A.18}$$

Here m_{nuc} is the mass of the nucleus, v is the halo velocity of the dark matter particle. S_{nuc} is the spin of the nucleus, μ_{nuc} is the magnetic dipole moment of the nucleus, and $F_D(E_r)$ is the dipole moment form factor for the nucleus. The dipole-charge interaction is clearly enhanced at low momentum transfer.

These results are only valid for the muon and the tau. However, in the case of

the electron, the only significant difference is that it is the scale associated with the momentum transfer in the process $|\vec{k}|$ that cuts off the logarithm in Eq. A.15, and not the mass of the lepton m_ℓ. In order to obtain approximate limits for the case of electron flavored dark matter it suffices to replace m_ℓ in Eq. A.15 by $|\vec{k}|$. We choose $|\vec{k}| = 10$ MeV as a reference value.

Bibliography

[1] Maxim Markevitch. Chandra observation of the most interesting cluster in the universe. 2005.

[2] Douglas Clowe, Marusa Bradac, Anthony H. Gonzalez, Maxim Markevitch, Scott W. Randall, et al. A direct empirical proof of the existence of dark matter. *Astrophys.J.*, 648:L109–L113, 2006.

[3] Observation of a new boson with a mass near 125 gev. Technical Report CMS-PAS-HIG-12-020, CERN, Geneva, Jul 2012.

[4] Observation of an excess of events in the search for the standard model higgs boson with the atlas detector at the lhc. Technical Report ATLAS-CONF-2012-093, CERN, Geneva, Jul 2012.

[5] E. Komatsu et al. Seven-Year Wilkinson Microwave Anisotropy Probe (WMAP) Observations: Cosmological Interpretation. *Astrophys.J.Suppl.*, 192:18, 2011.

[6] Alain Coc, Elisabeth Vangioni-Flam, Pierre Descouvemont, Abderrahim Adahchour, and Carmen Angulo. Updated Big Bang nucleosynthesis confronted to WMAP observations and to the abundance of light elements. *Astrophys.J.*, 600:544–552, 2004.

[7] V.C. Rubin, N. Thonnard, and Jr. Ford, W.K. Rotational properties of 21 SC galaxies with a large range of luminosities and radii, from NGC 4605 /R = 4kpc/ to UGC 2885 /R = 122 kpc/. *Astrophys.J.*, 238:471, 1980.

[8] Prateek Agrawal, Steve Blanchet, Zackaria Chacko, and Can Kilic. Flavored Dark Matter, and Its Implications for Direct Detection and Colliders. 2011.

[9] S.L. Glashow. Partial Symmetries of Weak Interactions. *Nucl.Phys.*, 22:579–588, 1961.

[10] Steven Weinberg. A Model of Leptons. *Phys.Rev.Lett.*, 19:1264–1266, 1967.

[11] Abdus Salam. Weak and Electromagnetic Interactions. *Conf.Proc.*, C680519:367–377, 1968.

[12] Palash B. Pal. Dirac, Majorana and Weyl fermions. 2010.

[13] Gerard 't Hooft. Renormalizable Lagrangians for Massive Yang-Mills Fields. *Nucl.Phys.*, B35:167–188, 1971.

[14] K. Nakamura et al. Review of particle physics. *J.Phys.G*, G37:075021, 2010.

[15] Nicola Cabibbo. Unitary Symmetry and Leptonic Decays. *Phys.Rev.Lett.*, 10:531–533, 1963.

[16] Makoto Kobayashi and Toshihide Maskawa. CP Violation in the Renormalizable Theory of Weak Interaction. *Prog.Theor.Phys.*, 49:652–657, 1973.

[17] S.L. Glashow, J. Iliopoulos, and L. Maiani. Weak Interactions with Lepton-Hadron Symmetry. *Phys.Rev.*, D2:1285–1292, 1970.

[18] Gino Isidori, Yosef Nir, and Gilad Perez. Flavor Physics Constraints for Physics Beyond the Standard Model. *Ann.Rev.Nucl.Part.Sci.*, 60:355, 2010.

[19] G. Hinshaw et al. Five-Year Wilkinson Microwave Anisotropy Probe (WMAP) Observations: Data Processing, Sky Maps, and Basic Results. *Astrophys.J.Suppl.*, 180:225–245, 2009.

[20] S. Perlmutter et al. Measurements of Omega and Lambda from 42 high redshift supernovae. *Astrophys.J.*, 517:565–586, 1999.

[21] Adam G. Riess et al. Observational evidence from supernovae for an accelerating universe and a cosmological constant. *Astron.J.*, 116:1009–1038, 1998.

[22] Adam G. Riess et al. Type Ia supernova discoveries at $z > 1$ from the Hubble Space Telescope: Evidence for past deceleration and constraints on dark energy evolution. *Astrophys.J.*, 607:665–687, 2004.

[23] Daniel J. Eisenstein et al. Detection of the baryon acoustic peak in the large-scale correlation function of SDSS luminous red galaxies. *Astrophys.J.*, 633:560–574, 2005.

[24] M. Kowalski et al. Improved Cosmological Constraints from New, Old and Combined Supernova Datasets. *Astrophys.J.*, 686:749–778, 2008.

[25] Alexey Boyarsky, Julien Lesgourgues, Oleg Ruchayskiy, and Matteo Viel. Lyman-alpha constraints on warm and on warm-plus-cold dark matter models. *JCAP*, 0905:012, 2009.

[26] Z. Ahmed et al. Dark Matter Search Results from the CDMS II Experiment. *Science*, 327:1619–1621, 2010.

[27] E. Aprile et al. The XENON100 Dark Matter Experiment. *Astropart.Phys.*, 35:573–590, 2012.

[28] D. Yu. Akimov, H.M. Araujo, E.J. Barnes, V.A. Belov, A. Bewick, et al. WIMP-nucleon cross-section results from the second science run of ZEPLIN-III. *Phys.Lett.*, B709:14–20, 2012.

[29] E. Armengaud et al. Final results of the EDELWEISS-II WIMP search using a 4-kg array of cryogenic germanium detectors with interleaved electrodes. *Phys.Lett.*, B702:329–335, 2011.

[30] G. Angloher, M. Bauer, I. Bavykina, A. Bento, C. Bucci, et al. Results from 730 kg days of the CRESST-II Dark Matter Search. *Eur.Phys.J.*, C72:1971, 2012.

[31] C.E. Aalseth et al. Results from a Search for Light-Mass Dark Matter with a P-type Point Contact Germanium Detector. *Phys.Rev.Lett.*, 106:131301, 2011.

[32] R. Bernabei et al. New results from DAMA/LIBRA. *Eur.Phys.J.*, C67:39–49, 2010.

[33] E. Behnke et al. Dark matter detection with bubble chambers. *Nucl.Phys.Proc.Suppl.*, 221:379, 2011.

[34] P. Benetti, R. Acciarri, F. Adamo, B. Baibussinov, M. Baldo-Ceolin, et al. First results from a Dark Matter search with liquid Argon at 87 K in the Gran Sasso Underground Laboratory. *Astropart.Phys.*, 28:495–507, 2008.

[35] S.C. Kim, H. Bhang, J.H. Choi, W.G. Kang, B.H. Kim, et al. New Limits on Interactions between Weakly Interacting Massive Particles and Nucleons Obtained with CsI(Tl) Crystal Detectors. *Phys.Rev.Lett.*, 108:181301, 2012.

[36] Anne M. Green. Astrophysical uncertainties on direct detection experiments. *Mod.Phys.Lett.*, A27:1230004, 2012.

[37] E. Aprile et al. First Dark Matter Results from the XENON100 Experiment. *Phys.Rev.Lett.*, 105:131302, 2010.

[38] Roberto Trotta, Farhan Feroz, Mike P. Hobson, Leszek Roszkowski, and Roberto Ruiz de Austri. The Impact of priors and observables on parameter inferences in the Constrained MSSM. *JHEP*, 0812:024, 2008.

[39] C. Savage, G. Gelmini, P. Gondolo, and K. Freese. Compatibility of DAMA/LIBRA dark matter detection with other searches. *JCAP*, 0904:010, 2009.

[40] Alex Geringer-Sameth and Savvas M. Koushiappas. Exclusion of canonical WIMPs by the joint analysis of Milky Way dwarfs with Fermi. *Phys.Rev.Lett.*, 107:241303, 2011.

[41] M. Ackermann et al. Constraining Dark Matter Models from a Combined Analysis of Milky Way Satellites with the Fermi Large Area Telescope. *Phys.Rev.Lett.*, 107:241302, 2011.

[42] Dan Hooper and Tim Linden. On The Origin Of The Gamma Rays From The Galactic Center. *Phys.Rev.*, D84:123005, 2011.

[43] Christoph Weniger. A Tentative Gamma-Ray Line from Dark Matter Annihilation at the Fermi Large Area Telescope. 2012.

[44] Meng Su and Douglas P. Finkbeiner. Strong Evidence for Gamma-ray Line Emission from the Inner Galaxy. 2012.

[45] O. Adriani et al. PAMELA results on the cosmic-ray antiproton flux from 60 MeV to 180 GeV in kinetic energy. *Phys.Rev.Lett.*, 105:121101, 2010.

[46] S.W. Barwick et al. Measurements of the cosmic ray positron fraction from 1-GeV to 50-GeV. *Astrophys.J.*, 482:L191–L194, 1997.

[47] M. Aguilar et al. Cosmic-ray positron fraction measurement from 1 to 30-GeV with AMS-01. *Phys.Lett.*, B646:145–154, 2007.

[48] J. Chang, J.H. Adams, H.S. Ahn, G.L. Bashindzhagyan, M. Christl, et al. An excess of cosmic ray electrons at energies of 300-800 GeV. *Nature*, 456:362–365, 2008.

[49] M. Ackermann et al. Measurement of separate cosmic-ray electron and positron spectra with the Fermi Large Area Telescope. *Phys.Rev.Lett.*, 108:011103, 2012.

[50] Stefano Profumo. Dissecting cosmic-ray electron-positron data with Occam's Razor: the role of known Pulsars. *Central Eur.J.Phys.*, 10:1–31, 2011.

[51] R. Abbasi et al. Multi-year search for dark matter annihilations in the Sun with the AMANDA-II and IceCube detectors. *Phys.Rev.*, D85:042002, 2012.

[52] T. Tanaka et al. An Indirect Search for WIMPs in the Sun using 3109.6 days of upward-going muons in Super-Kamiokande. *Astrophys.J.*, 742:78, 2011.

[53] Prateek Agrawal, Zackaria Chacko, Can Kilic, and Rashmish K. Mishra. Direct Detection Constraints on Dark Matter Event Rates in Neutrino Telescopes, and Collider Implications. 2010.

[54] Serguei Chatrchyan et al. Search for Dark Matter and Large Extra Dimensions in pp Collisions Yielding a Photon and Missing Transverse Energy. 2012.

[55] R.D. Peccei and Helen R. Quinn. CP Conservation in the Presence of Instantons. *Phys.Rev.Lett.*, 38:1440–1443, 1977.

[56] R.D. Peccei and Helen R. Quinn. Constraints Imposed by CP Conservation in the Presence of Instantons. *Phys.Rev.*, D16:1791–1797, 1977.

[57] Steven Weinberg. A New Light Boson? *Phys.Rev.Lett.*, 40:223–226, 1978.

[58] Frank Wilczek. Problem of Strong p and t Invariance in the Presence of Instantons. *Phys.Rev.Lett.*, 40:279–282, 1978.

[59] Jihn E. Kim. Weak Interaction Singlet and Strong CP Invariance. *Phys.Rev.Lett.*, 43:103, 1979.

[60] Mikhail A. Shifman, A.I. Vainshtein, and Valentin I. Zakharov. Can Confinement Ensure Natural CP Invariance of Strong Interactions? *Nucl.Phys.*, B166:493, 1980.

[61] Michael Dine, Willy Fischler, and Mark Srednicki. A Simple Solution to the Strong CP Problem with a Harmless Axion. *Phys.Lett.*, B104:199, 1981.

[62] A.R. Zhitnitsky. THE WEINBERG MODEL OF THE CP VIOLATION AND T ODD CORRELATIONS IN WEAK DECAYS. (IN RUSSIAN). *Sov.J.Nucl.Phys.*, 31:529–534, 1980.

[63] John Preskill, Mark B. Wise, and Frank Wilczek. Cosmology of the Invisible Axion. *Phys.Lett.*, B120:127–132, 1983.

[64] L.F. Abbott and P. Sikivie. A Cosmological Bound on the Invisible Axion. *Phys.Lett.*, B120:133–136, 1983.

[65] Michael Dine and Willy Fischler. The Not So Harmless Axion. *Phys.Lett.*, B120:137–141, 1983.

[66] P. Sikivie. DETECTION RATES FOR 'INVISIBLE' AXION SEARCHES. *Phys.Rev.*, D32:2988, 1985.

[67] S.J. Asztalos et al. A SQUID-based microwave cavity search for dark-matter axions. *Phys.Rev.Lett.*, 104:041301, 2010.

[68] Asimina Arvanitaki, Savas Dimopoulos, Sergei Dubovsky, Nemanja Kaloper, and John March-Russell. String Axiverse. *Phys.Rev.*, D81:123530, 2010.

[69] Peter W. Graham and Surjeet Rajendran. Axion Dark Matter Detection with Cold Molecules. *Phys.Rev.*, D84:055013, 2011.

[70] Luis E. Ibanez. The Scalar Neutrinos as the Lightest Supersymmetric Particles and Cosmology. *Phys. Lett.*, B137:160, 1984.

[71] John R. Ellis, J. S. Hagelin, Dimitri V. Nanopoulos, Keith A. Olive, and M. Srednicki. Supersymmetric relics from the big bang. *Nucl. Phys.*, B238:453–476, 1984.

[72] John S. Hagelin, Gordon L. Kane, and S. Raby. Perhaps Scalar Neutrinos Are the Lightest Supersymmetric Partners. *Nucl. Phys.*, B241:638, 1984.

[73] Mark W. Goodman and Edward Witten. Detectability of certain dark-matter candidates. *Phys. Rev.*, D31:3059, 1985.

[74] Katherine Freese. Can Scalar Neutrinos Or Massive Dirac Neutrinos Be the Missing Mass? *Phys. Lett.*, B167:295, 1986.

[75] Toby Falk, Keith A. Olive, and Mark Srednicki. Heavy Sneutrinos as Dark Matter. *Phys. Lett.*, B339:248–251, 1994.

[76] John March-Russell, Christopher McCabe, and Matthew McCullough. Neutrino-Flavoured Sneutrino Dark Matter. *JHEP*, 1003:108, 2010.

[77] Geraldine Servant and Timothy M. P. Tait. Is the lightest Kaluza-Klein particle a viable dark matter candidate? *Nucl. Phys.*, B650:391–419, 2003.

[78] Jennifer Kile and Amarjit Soni. Flavored Dark Matter in Direct Detection Experiments and at LHC. *Phys.Rev.*, D84:035016, 2011.

[79] Jernej F. Kamenik and Jure Zupan. Discovering Dark Matter Through Flavor Violation at the LHC. *Phys.Rev.*, D84:111502, 2011.

[80] Yanou Cui, Lisa Randall, and Brian Shuve. Emergent Dark Matter, Baryon, and Lepton Numbers. *JHEP*, 1108:073, 2011.

[81] Brian Batell, Josef Pradler, and Michael Spannowsky. Dark Matter from Minimal Flavor Violation. *JHEP*, 1108:038, 2011.

[82] G. D'Ambrosio, G. F. Giudice, G. Isidori, and A. Strumia. Minimal flavour violation: An effective field theory approach. *Nucl. Phys.*, B645:155–187, 2002.

[83] Matthew J. Strassler and Kathryn M. Zurek. Echoes of a hidden valley at hadron colliders. *Phys. Lett.*, B651:374–379, 2007.

[84] Joachim Kopp, Viviana Niro, Thomas Schwetz, and Jure Zupan. DAMA/LIBRA and leptonically interacting Dark Matter. *Phys. Rev.*, D80:083502, 2009.

[85] Gintaras Duda, Ann Kemper, and Paolo Gondolo. Model independent form factors for spin independent neutralino nucleon scattering from elastic electron scattering data. *JCAP*, 0704:012, 2007.

[86] Spencer Chang, Neal Weiner, and Itay Yavin. Magnetic Inelastic Dark Matter. *Phys. Rev.*, D82:125011, 2010.

[87] E. Aprile et al. Dark Matter Results from 100 Live Days of XENON100 Data. *Phys.Rev.Lett.*, 107:131302, 2011.

[88] Marco Cirelli, Nicolao Fornengo, and Alessandro Strumia. Minimal dark matter. *Nucl. Phys.*, B753:178–194, 2006.

[89] Prateek Agrawal, Zackaria Chacko, Can Kilic, and Rashmish K. Mishra. A Classification of Dark Matter Candidates with Primarily Spin-Dependent Interactions with Matter. 2010.

[90] David B. Kaplan and Aneesh Manohar. Strange Matrix Elements in the Proton from Neutral Current Experiments. *Nucl. Phys.*, B310:527, 1988.

[91] Xiang-dong Ji and D. Toublan. Heavy-quark contribution to the proton's magnetic moment. *Phys. Lett.*, B647:361–365, 2007.

[92] JiJi Fan, Matthew Reece, and Lian-Tao Wang. Non-relativistic effective theory of dark matter direct detection. *JCAP*, 1011:042, 2010.

[93] Fabio Maltoni and Tim Stelzer. MadEvent: Automatic event generation with MadGraph. *JHEP*, 02:027, 2003.

[94] Johan Alwall et al. MadGraph/MadEvent v4: The New Web Generation. *JHEP*, 09:028, 2007.

[95] Patrick Meade and Matthew Reece. BRIDGE: Branching ratio inquiry / decay generated events. 2007.

[96] Torbjorn Sjostrand, Stephen Mrenna, and Peter Z. Skands. PYTHIA 6.4 Physics and Manual. *JHEP*, 05:026, 2006.

[97] John Conway et al. *PGS 4: Pretty Good Simulation of high energy collisions*, 2006.

[98] Susy searches at atlas in multilepton final states with jets and missing transverse energy. Technical Report ATLAS-CONF-2011-039, CERN, Geneva, Mar 2011.

[99] Serguei Chatrchyan et al. Search for Physics Beyond the Standard Model Using Multilepton Signatures in pp Collisions at sqrt(s)=7 TeV. 2011.

[100] G. L. Bayatian et al. CMS technical design report, volume II: Physics performance. *J. Phys.*, G34:995–1579, 2007.

[101] Mihoko M. Nojiri, Yasuhiro Shimizu, Shogo Okada, and Kiyotomo Kawagoe. Inclusive transverse mass analysis for squark and gluino mass determination. *JHEP*, 06:035, 2008.

[102] Mihoko M. Nojiri, Kazuki Sakurai, Yasuhiro Shimizu, and Michihisa Takeuchi. Handling jets + missing E_T channel using inclusive mT2. *JHEP*, 10:100, 2008.

[103] Kaustubh Agashe, Doojin Kim, Devin G. E. Walker, and Lijun Zhu. Using M_T2 to Distinguish Dark Matter Stabilization Symmetries. 2010.

[104] Arvind Rajaraman and Felix Yu. A New Method for Resolving Combinatorial Ambiguities at Hadron Colliders. *Phys. Lett.*, B700:126–132, 2011.

[105] Yang Bai and Hsin-Chia Cheng. Identifying Dark Matter Event Topologies at the LHC. *JHEP*, 06:021, 2011.

[106] Vernon Barger, Wai-Yee Keung, and Danny Marfatia. Electromagnetic properties of dark matter: dipole moments and charge form factor. *Phys. Lett.*, B696:74–78, 2011.